Metamaterial-Based Efficient Electrically Small Antennas

Richard W. Ziolkowski, *Fellow, IEEE*, and Aycan Erentok

***Abstract*—A metamaterial paradigm for achieving an efficient, electrically small antenna is introduced. Spherical shells of homogenous, isotropic negative permittivity (ENG) material are designed to create electrically small resonant systems for several antennas: an infinitesimal electric dipole, a very short center-fed cylindrical electric dipole, and a very short coaxially-fed electric monopole over an infinite ground plane. Analytical and numerical models demonstrate that a properly designed ENG shell provides a distributed inductive element resonantly matched to these highly capacitive electrically small antennas, i.e., an ENG shell can be designed to produce an electrically small system with a zero input reactance and an input resistance that is matched to a specified source resistance leading to overall efficiencies approaching unity. Losses and dispersion characteristics of the ENG materials are also included in the analytical models. Finite element numerical models of the various antenna-ENG shell systems are developed and used to predict their input impedances. These electrically small antenna-ENG shell systems with idealized dispersionless ENG material properties are shown to be very efficient and to have fractional bandwidths above the values associated with the Chu limit for the quality factor without any degradation in the radiation patterns of the antennas. Introducing dispersion and losses into the analytical models, the resulting bandwidths are shown to be reduced significantly, but remain slightly above (below) the corresponding Chu-based value for an energy-based limiting (Drude) dispersion model of the permittivity of the ENG shell.**

***Index Terms*—antenna theory, Chu limit, complex media, electrically small antennas, electromagnetic theory, metamaterials.**

I. Introduction

HISTORICALLY, there has been much interest in electrically small antennas [1]–[34]. Antennas that are electrically small, efficient, and have significant bandwidth would fill many needs if antenna engineers could reconcile these usually contradictory requirements. This is especially true recently with increased uses of wireless technologies for communications and sensor networks.

It is well known that an electrically small electric dipole antenna is an inefficient radiator, i.e., because it has a very small radiation resistance while simultaneously having a very large capacitance reactance, a large impedance mismatch to any realistic power source exists [1]–[18]. Consequently, to obtain a high overall efficiency, considerable effort must be expended on a matching network that produces an impedance that is conjugately matched to the dipole's impedance; i.e., it forces the total reactance to zero by introducing a very large inductive reactance which cancels the very large capacitive reactance of the electrically small electric dipole, and that then matches this resonant system to a feed network, e.g., forces the input resistance of this resonant system to 50 Ω. Generally, this matching method utilizes passive lumped elements, although approaches with active elements have also been considered, for instance, in [19]. Because of the very large reactance values involved, these matched resonant systems generally have very narrow bandwidths, imperfect efficiencies, and high tolerance requirements for their fabrication.

Since their potential impact is large, there has been a resurgence of interest in electrically small antenna technologies. The well known Chu result [1]–[18] defines a limit for the radiation quality factor and, hence, bandwidth of an electrically small antenna, which can be enclosed within a sphere of effective radius r_e. The quality factor approaches this Chu limit only if the antenna efficiently utilizes the available volume within that radiation sphere. There have been a wide variety of recent approaches to achieve this goal including clever packing of resonant antenna elements into this small volume using natural geometrical configurations [12]–[15], fractal curve antennas [20]–[23] and space-filling curve antennas [24]–[27]. Very non-intuitive structures generated with optimization approaches have also been considered successfully [28].

A different paradigm for achieving an efficient electrically small antenna (EESA) that has interesting bandwidth characteristics is reported in this paper. It is based on the incorporation of metamaterials with negative permittivity medium properties into the antenna system. Throughout, to simplify the discussion, we will consider an electrically small electric dipole as the basic antenna element. We consider the integration of such an antenna with a metamaterial to simultaneously achieve large overall efficiency and large fractional bandwidth (FBW). This integration is based on the electric dipole—double negative (DNG) and single negative (SNG) spherical shell systems considered in [29]–[34]. Basically, as suggested in [30]–[33], we will use an epsilon-negative (ENG) shell as a distributed matching element to the electric dipole rather than a passive or active "lumped" element to achieve this goal. The analytical model of an ideal infinitesimal electric dipole antenna radiating in the presence of an ENG shell that was developed in [29]–[33] will be used to demonstrate the theoretical results. In particular, the fact that an electrically small ENG shell can be designed to have a natural resonance and it can be driven by the electrically small electric dipole to enhance significantly the power radiated into the far field, is emphasized. In addition

Manuscript received June 30, 2005; revised January 17, 2006. This work was supported in part by DARPA Contract HR0011-05-C-0068 and by ONR under Contract 14-04-1-0320.

The authors are with the Department of Electrical and Computer Engineering, The University of Arizona, Tucson, AZ 85721-0104 USA (e-mail: ziolkowski@ece.arizona.edu; erentoka@ece.arizona.edu).

Digital Object Identifier 10.1109/TAP.2006.877179

to analyzing the performance of the ideal source case, we will then consider a simulation model of a realistic center-fed cylindrical electric dipole within the ENG shell using ANSOFT's High Frequency Structure Simulator (HFSS) to confirm the analytical model's results and to obtain an accurate calculation of the overall efficiency of this dipole-ENG shell system. It will be demonstrated that the electrically small, center-fed electric dipole-ENG shell system can also be designed to produce a naturally resonant configuration. It is further demonstrated that the dimensions of the ENG shell and the electric dipole antenna can be adjusted to produce a resonant configuration whose overall efficiency approaches unity, i.e., one whose total reactance is zero and whose resistance is matched to the feed line to achieve a high overall efficiency and, hence, a maximum in the radiated power. Moreover, when the negative permittivity is treated as dispersionless, it is shown that this system has a FBW much larger than that predicted by the Chu limit. These ideal (dispersionless) resonant designs are further studied using a coaxially-fed monopole-ENG hemispherical shell system. Discussion of the behavior of these antenna-ENG shell systems in the non-ideal case in which material dispersion and losses play a significant role will also be given analytically, particularly in respect to their frequency bandwidth. It is shown that when dispersion and losses are introduced into the analytical models, the resulting bandwidths are reduced significantly, but remain slightly above (below) the corresponding Chu-based value for an energy-based limiting (Drude) dispersion model of the permittivity of the ENG shell.

We note that the ENG shell may be realized artificially with metamaterials or naturally with plasmas. In fact, the basic dipole-shell configuration has a long history for both source and scattering applications [35]–[39]. The source problem when the shell is a plasma was of particular interest in the beginnings of the space program. In contrast to previous considerations of this problem, the work presented here emphasizes resonant configurations that exist even when the system is electrically small. Negative permittivity metamaterial element designs to achieve the requisite properties discussed below are in progress and are beyond the scope of this presentation. The focus of this paper is the theoretical basis for the metamaterial paradigm; proof-of-concept experiments are in progress, and their results will be reported elsewhere.

As a matter of definitions to be used throughout this paper, an $\exp(+j\omega t)$ time dependence is assumed throughout. As proposed by Best in [13], an electrically small antenna in free space is defined by the constraint that $kr_e \leq 0.5$, where the free space wavelength $\lambda = c/f$, f being the frequency of operation and c is the speed of light, and $k = 2\pi/\lambda$ is the corresponding wave vector. Thus, for the target frequency of interest here, $f_0 = \omega_0/2\pi = 300$ MHz, the free space wavelength $\lambda_0 = 1.0$ m; and, consequently, the effective radius must be smaller than the value $r_e = 0.5/(2\pi) = 7.958\,\mathrm{cm} = 79.58\,\mathrm{mm}$ to meet this criterion. Note that this is half of the Wheeler radiansphere value $r_W = 1/(2\pi)$, which is a qualitative measure of the boundary between the near field and the far field of an electrically small antenna. The infinitesimal electric dipole, in all of the analytic cases, and the current source center-fed dipole are driven with a 1.0 A current across their terminals; the more realistic center-fed dipole and coaxially-fed monopole antennas are driven with a 1.0 W input power in all of the numerical cases.

We note that there are two types of resonances discussed in this paper. The natural resonance associated with the system geometry occurs where the determinant of the scattering matrix approaches zero; i.e., because the analytical solution is of the form $E = M_s^{-1}F$, where F is the driving field expansion coefficient array, E is the scattered field expansion coefficient array, and M_s is the matrix of the modal terms obtained from enforcement of the electromagnetic boundary conditions across the interfaces, a natural resonance occurs when $\det(M_s) \to 0$. An antenna resonance (anti-resonance) occurs where the reactance goes to zero and its derivative with respect to the frequency is positive (negative); i.e., if one considers a simple series LRC circuit representing the antenna, its response is resonant when the reactance goes to zero at $\omega_{\mathrm{res}} = 1/\sqrt{LC}$.

We begin with dipole-metamaterial shell system designs based upon idealized dispersionless metamaterials. This approach allows us to explain the behavior of these designs without any additional complications. It also makes the HFSS simulation requirements more manageable. As will be shown, dispersion significantly impact the bandwidth results, but not the peak radiated power values. While dispersive metamaterial models are readily incorporated into the analytical solutions, their corresponding frequency resolution demands on the detailed HFSS simulations are severe. The dispersionless metamaterial-based HFSS models, which provide information not available from the analytical solutions, establish the ability of the analytical models to accurately predict the radiated power performance and to establish bounds on the bandwidth properties of the dipole-metamaterial shell systems considered.

II. Infinitesimal Electric Dipole Antenna Surrounded by an ENG Shell: Analytical Results

It has been demonstrated in [30]–[33] that an infinitesimal electric dipole-ENG shell system will show similar resonance characteristics to those exhibited by the corresponding electric dipole-DNG shell system [29], [34]. As in [18], the term "infinitesimal electric dipole" denotes an electric dipole whose length $\ell \ll \lambda$. This shell geometry is shown in Fig. 1. This configuration and the solution formulation are the same as the one presented in [29]. However, we now allow for the presence of losses in the various regions. The resulting analytical solutions were implemented numerically as discussed in [29]–[34]. The electric dipole is located in the homogeneous spherical Region 1 defined for $0 < r < r_1$ with the constant permittivity and permeability ε_1, μ_1. The spherical shell, Region 2, has constant permittivity and permeability ε_2, μ_2 and has an inner radius r_1 and outer radius r_2. Region 3 has the constant permittivity and permeability ε_3, μ_3; it is defined between outer radius r_2 and infinity. The electric dipole is oriented along the z-axis.

A. Electric Dipole-ENG Shell System Without Dispersion

First consider the inner sphere, Region 1, and the outer region, Region 3, to be free space, a double positive (DPS) medium, with $\varepsilon_1, \varepsilon_3 = \varepsilon_0$ and $\mu_1, \mu_3 = \mu_0$, where ε_0 and μ_0 are, respectively, the free space permittivity and permeability values. The spherical ENG shell, Region 2, is described by the material

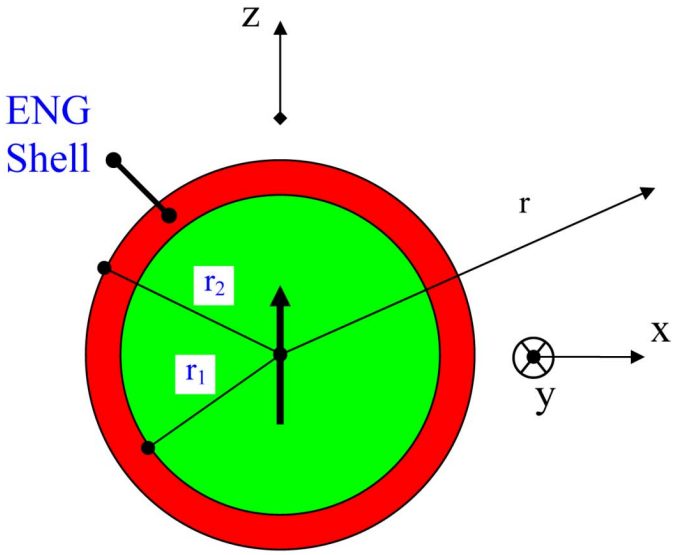

Fig. 1. Geometry of the z-oriented electric dipole-ENG shell system.

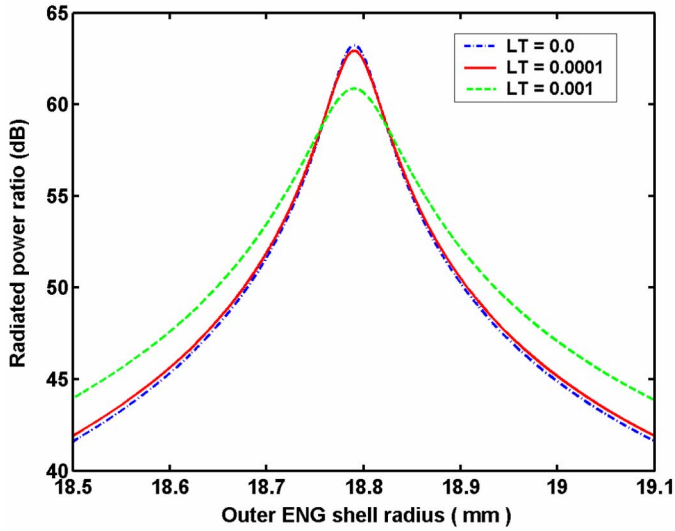

Fig. 2. Radiated power for a $\ell = 10$ mm infinitesimal electric dipole in $r_1 = 10$ mm ENG shells with a frequency independent relative permittivity $\varepsilon_r = -3.0$ having different loss tangents normalized by the power radiated by the same infinitesimal electric dipole in free space.

constants: $\varepsilon_2 = \varepsilon_r\varepsilon_0 - j\varepsilon_{im}$, where $\varepsilon_r < 0$ and $\varepsilon_{im} > 0$, and $\mu = \mu_0$. The loss tangent is thus given by $LT = \varepsilon_{im}/|\varepsilon_r\varepsilon_0|$. Consequently, the infinitesimal electric dipole is located in the free space spherical Region 1, and the power radiated by the electric dipole-ENG shell system propagates in free space. First, we define a parameter that will enable us to quantify the infinitesimal electric dipole-ENG system's far-field radiated power characteristics for different ENG medium shell sizes and permittivity values, i.e., the radiated power ratio (RPR)

$$\mathrm{RPR} = 10\log_{10}\left[\frac{\mathrm{P}_{\text{with shell}}(1\text{ A input current})}{\mathrm{P}_{\text{without shell}}(1\text{ A input current})}\right]\ (\mathrm{dB}). \tag{1}$$

The total length of the infinitesimal electric dipole is assumed to be $\ell = 10.0$ mm $= \lambda_0/100$. With $\varepsilon_r = -3.0$ and $r_1 = 10.0$ mm, the RPRs of the infinitesimal electric dipole-ENG shell system as a function of the outer radius r_2 for the lossless case with $LT = 0.0$, and the lossy cases with $LT = 0.0001, 0.001$, are shown in Fig. 2. The lossless case has its maximum RPR at $r_{2,\max} = 18.79$ mm. This demonstrates as discussed in [29]–[34] that the infinitesimal electric dipole-ENG shell system has a natural resonance even though it is electrically small, i.e., $k_0 r_{2,\max} = 0.118$. Because it is a resonant configuration, the presence of losses lowers the peak RPR and broadens the resonance. The magnitude of the real part of the total electric field distribution and of the real part of the total magnetic field distribution for the resonant lossless ENG shell case, i.e., with $r_1 = 10$ mm and $r_2 = 18.79$ mm, are shown in Fig. 3(a) and (b), respectively. From these field distributions it is clear that the maximum power is radiated broadside to the radiating element.

Because of their small sizes, the inner sphere and the ENG shell act as electrically small electric dipole radiators. Thus, the electric dipole and inner sphere act as capacitive elements. However, because the material in it is an ENG medium, the shell acts as an inductive element. This behavior is depicted in Fig. 4. We can introduce an effective reactance to describe the behavior of the ENG shell at the driving frequency; which is approximately proportional to the expression

$$X_{\text{shell}} = \frac{1}{j\omega_0 C_{\text{shell}}} = j\omega_0 L_{\text{eff}} \propto j\omega_0 \frac{1}{\omega_0^2|\varepsilon|\Delta r} \tag{2}$$

where Δr is the thickness of the ENG shell. The reactance is positive and, hence, the electrically small ENG shell represents an inductive element. The effective inductance depends on the magnitude of the permittivity of the shell, the shell thickness, and the driving frequency. When the electrically small electric dipole antenna, a capacitive element, radiates in the presence of this inductive ENG shell, an *LC* resonator is formed. The corresponding resonant frequency is approximately proportional to the expression

$$\omega_{\text{res}} = \frac{1}{\sqrt{L_{\text{eff}}C_{\text{eff}}}} \propto \omega_0\sqrt{\frac{|\varepsilon|\Delta r}{C_{\text{eff}}}} \tag{3}$$

where C_{eff} is taken to be the effective capacitance of the electric dipole antenna and the inner shell region.

For a fixed inner radius, excitation frequency, and negative epsilon, the variation in the outer shell radius, r_2, then tunes this *LC* system through the resonance. A more negative relative permittivity requires a corresponding decrease in the thickness of the shell to maintain the resonance frequency at a particular value for a specified driving frequency. This behavior is demonstrated explicitly in Fig. 5. The RPRs for the corresponding lossless cases for $\varepsilon_r = -2.9$ and $\varepsilon_r = -3.1$ as functions of the outer radius for $r_1 = 10$ mm are compared with the $\varepsilon_r = -3.0$ lossless case in Fig. 2. In all cases, the electric dipole has the length $\ell = 10$ mm. As the relative permittivity increases (decreases),

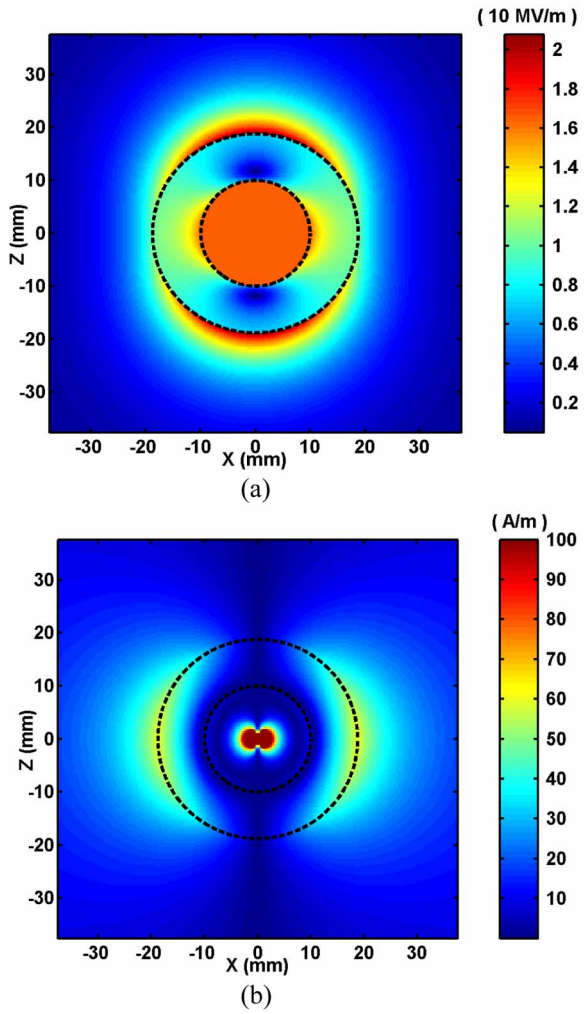

Fig. 3. Electric (a) and magnetic field (b) distributions for a $\ell = 10$ mm z-oriented infinitesimal electric dipole in the resonant $r_1 = 10$ mm, $r_2 = 18.79$ mm lossless ENG shell with a frequency independent relative permittivity $\varepsilon_r = -3.0$.

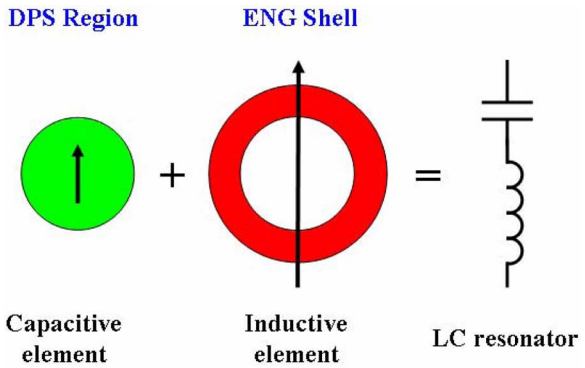

Fig. 4. The antenna and the surrounding DPS (free space) region act as an electrically small electric dipole; hence, it acts as a capacitive element. The surrounding ENG shell, once excited by the electric dipole antenna, also acts as an electrically small electric dipole. However, this capacitive element, because of the presence of the negative permittivity, acts as an inductive element. The combined system thus forms an *LC* resonator.

the peak of the RPR occurs at a decreasing (increasing) outer radius, hence, thinner (thicker) ENG shell.

This behavior was confirmed further with comparisons between the corresponding analytical ENG and DNG shell cases.

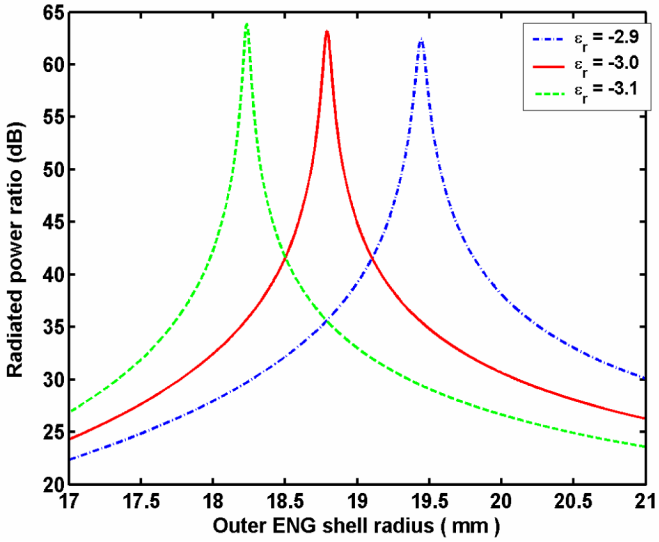

Fig. 5. Radiated power for a $\ell = 10$ mm infinitesimal electric dipole in $r_1 = 10$ mm lossless ENG shells having different frequency independent negative permittivities normalized by the power radiated by the same infinitesimal electric dipole in free space.

The resonant DNG shell case occurs for $r_{2,\max} = 18.69$ mm rather than at $r_{2,\max} = 18.79$ mm. The smaller outer radius value occurs because the inductance of the DNG shell with a negative permeability acts as another capacitance that is in series with the electric dipole-inner sphere capacitance, thus decreasing the total capacitance. As indicated by (3), a decrease in the shell thickness would be required to maintain the resonant frequency.

Consider the $\ell = 10$ mm infinitesimal electric dipole surrounded by the ENG shell with $r_1 = 10$ mm and $r_2 = 18.79$ mm and with $\varepsilon_r = -3.0$ and the loss tangents considered in Fig. 2. The RPR as a function of the driving frequency is shown in Fig. 6. If $f_{+,3\text{ dB}}$ and $f_{-,3\text{ dB}}$ represent the frequencies above and below the resonance frequency where the RPR falls to half its peak value, the FBW is related to the radiation quality factor, Q_{BW}, by the relation [18]

$$\text{FBW} = \frac{\Delta f_{3\text{ dB}}}{f_{0\text{ dB}}} = \frac{1}{Q_{\text{BW}}} \tag{4}$$

where $\Delta f_{3\text{ dB}} = f_{+,3\text{ dB}} - f_{-,3\text{ dB}}$. This relationship between the 1/2-RPR bandwidth and the Q in the range of frequencies near the resonance of this analytical system is acceptable because the source current driving the infinitesimal electric dipole antenna is constant and independent of the frequency. It is valid as long as the FBW is not too large [18, p. 639]. From Fig. 6 one finds for the lossless case that $f_{-3\text{ dB}} = 281.32$ MHz and $f_{+3\text{ dB}} = 312.41$ MHz and the peak value 63.35 dB occurs at $f_{0\text{ dB}} = 297.30$ MHz, slightly offset from the target frequency. Thus, the lossless infinitesimal electric dipole-ENG shell system has the $\text{FBW}_{\text{ENG}} = 10.46\%$ and the quality factor $Q_{\text{BW,ENG}} = 9.56$. Note that the slight offset in frequency implies that the ENG shell could be further tuned so that the frequency dependence is centered on $f_0 = 300$ MHz. Calculations show that an ENG shell with $r_1 = 10$ mm and $r_2 =$

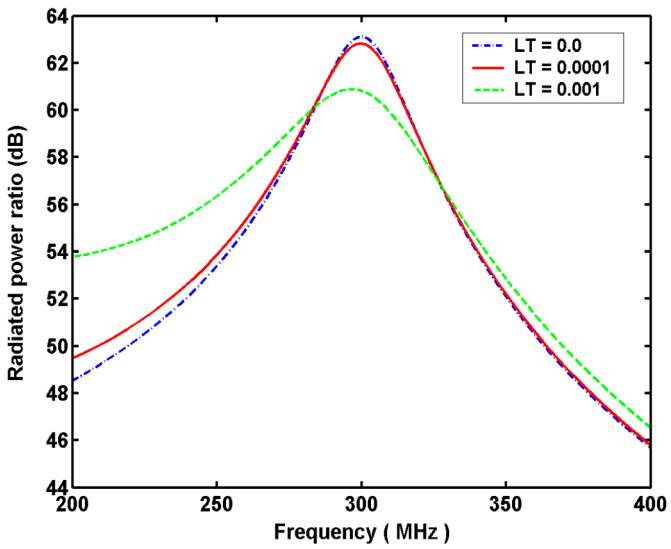

Fig. 6. Frequency dependence of the radiated power for a $\ell = 10$ mm infinitesimal electric dipole in lossless and lossy $r_1 = 10$ mm, $r_2 = 18.79$ mm ENG shells with a frequency independent relative permittivity $\varepsilon_r = -3.0$ normalized by the power radiated by the same infinitesimal electric dipole in free space.

18.7944 mm and with $\varepsilon_r = -3.0$ has its frequency response centered at f_0.

The minimum radiation quality factor for an electrically small electric dipole antenna, the so-called Chu limit, is known to be [1], [11], [18]

$$Q_{\text{Chu limit}} = \frac{1 + 2(k_0 r_e)^2}{(k_0 r_e)^3 \left[1 + (k_0 r_e)^2\right]} \tag{5}$$

when the electric dipole radiates into free space. This means $Q_{\text{Chu limit}} \approx 1/(k_0 r_e)^3$ for $k_0 r_e \ll 1$. Consequently, as its electrical size decreases, the radiation quality factor for the electric dipole antenna in free space increases dramatically, causing a corresponding decrease in the FBW of the antenna. With $f_{0\text{ dB}} = 297.30$ MHz and $r_e = r_{2,\max} = 18.79$ mm, the electrical size of the lossless case is $k_{0\text{ dB}} r_e = 0.117$, which means that the quality factor predicted for this electrically small antenna system is $Q_{\text{Chu limit}} = 632.83$. Consequently, the quality factor obtained for the lossless infinitesimal electric dipole-ENG shell system is substantially smaller than the Chu limiting value: $Q_{\text{BW,ENGshell}} = 0.015 Q_{\text{Chu limit}}$. We note that this result does not include dispersion, a significant issue that will be addressed in Section V.

III. Electrically Small Electric Dipole Antenna Surrounded by an ENG Shell: HFSS Results

Because the analytical models do not include any properties of a feed network, they do not provide critical information concerning the input impedance of a realistic dipole-ENG shell system. Moreover, because the RPR results for the infinitesimal electric dipole-ENG shell cases are equivalent to an increase in the corresponding radiation resistance, one might conclude that there would be a huge mismatch between that system and a feed network making our structure useless in practice. On the other hand, if our physical description of the interaction between the infinitesimal electric dipole antenna and the ENG shell is correct, then we should be able to match the inductive ENG shell with a realistic electrically small electric dipole antenna to achieve a resonant system. To characterize the behavior of a more realistic electric dipole-ENG shell system, we have modeled an electrically small center-fed cylindrical electric dipole antenna that is centered in an ENG spherical shell using HFSS. The details of the HFSS simulation models used in this study are described in the Appendix. A constant current source model was first used to verify the analytical results and a lumped element model was used to obtain the input impedance of the more realistic electric dipole-ENG shell system.

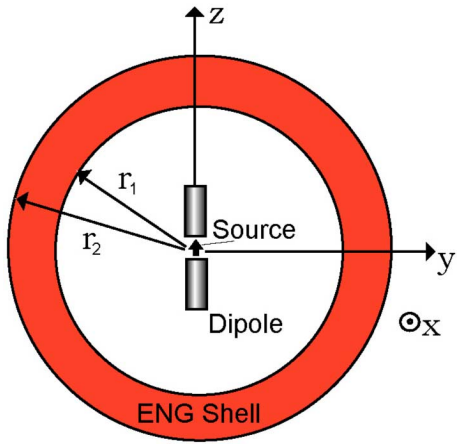

Fig. 7. HFSS model of the z-oriented electric dipole-ENG shell system.

A. Electric Dipole-ENG Shell System Using a Current Source Model at 300 MHz

The constant current source results were first tested with the HFSS model by considering the center-fed cylindrical electric dipole antenna radiating in free space. This center-fed cylindrical electric dipole antenna was defined in HFSS using two identical perfect electric conductor (PEC) circular cylinders that were separated by a vacuum gap, another circular cylinder. The antenna length was $\ell = 10$ mm; the length of the vacuum gap was 0.2 mm. The radius of the cylindrical antenna was $r_{\text{antenna}} = 0.06$ mm $= \lambda_0/16666$; hence, the diameter of the gap was 0.12 mm. Note that these choices produced a high aspect ratio with $\ell/(2r_{\text{antenna}}) = 83.33$. The computed free space radiated power and the corresponding maximum directivity results were, respectively, only 4.3% and 4.0% different from the approximate analytical results computed with the relations given in Balanis [18, pp. 566–570], thus validating this HFSS constant current electric dipole model in free space. A sketch of the HFSS electric dipole-ENG shell system model is shown in Fig. 7.

Next, the constant current source, center-fed electric dipole-ENG shell system at 300 MHz was modeled. An ENG shell with a frequency independent $(\varepsilon, \mu) = (-3\varepsilon_0, +\mu_0)$ and $r_1 = 10$ mm that was centered on the electric dipole was introduced. This HFSS model corresponds directly to the model of the analytical infinitesimal electric dipole-ENG shell system. With the properly specified numerical model discussed

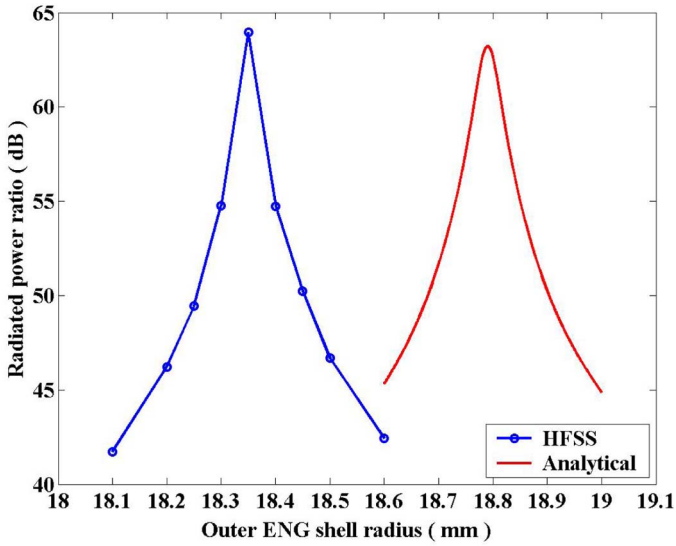

Fig. 8. Comparison of the power radiated by the analytical infinitesimal electric dipole-ENG shell system and the corresponding HFSS constant current source center-fed electric dipole model at 300 MHz for an inner radius $r_1 = 10.0\,\mathrm{mm}$ ENG shell with a frequency independent relative permittivity $\varepsilon_r = -3.0$ normalized by the values for the same electric dipole radiating in free space.

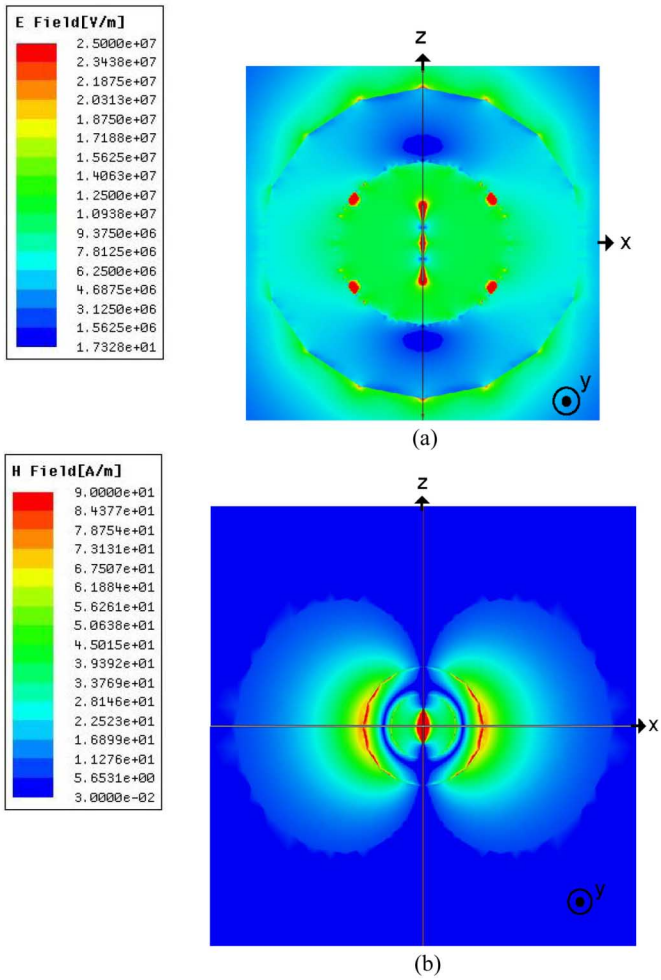

Fig. 9. Electric (a) and magnetic field (b) distributions of the resonant HFSS constant current z-oriented center-fed electric dipole-ENG shell system designed at 300 MHz with $r_1 = 10.0\,\mathrm{mm}$, $r_2 = 18.35\,\mathrm{mm}$, and a frequency independent relative permittivity $\varepsilon_r = -3.0$.

in the Appendix, the HFSS simulations of the predicted the RPR shown in Fig. 8. The peak of the RPR curve, 63.97 dB, occurs at the outer radius $r_{2,\max} = 18.35\,\mathrm{mm}$. Thus, the HFSS constant current source, center-fed electric dipole-ENG shell system shows a RPR and resonant spherical shell size very similar to the analytical results, given again in Fig. 8. Note that each red circle in Fig. 8 represents an individual HFSS simulation; these results are almost perfectly symmetric about the resonant outer radius value further supporting the consistency of these simulations. A comparison of the analytical and HFSS simulation results in Fig. 8 indicates a slight shift of the resonant shell size. This is due to the perturbations introduced by the finite radius wire antenna. In particular, the realistic antenna changes the capacitance to which the ENG shell must be matched. The analytical RPR curve shown in Fig. 8 simply demonstrates the case where the ENG shell matches the capacitance introduced only by the very small electrical length of the antenna. The required matching inductance for this ideal case is smaller than the value needed in the realistic antenna case where an extra capacitance is introduced by the finite radius of the antenna and the gap feed. The ENG shell size in the infinitesimal electric dipole case is thus larger than in the realistic antenna-ENG shell system as the required amount of matching inductance is smaller. Because of the presence of the vacuum gap, finite antenna radius, and the numerical imperfections of the spherical shells and the numerical solution process, the very good agreement between the analytical and numerical results validate both and provide us with an indication of the sensitivity of the analytical results to such perturbations.

Comparisons of the total E- and H-field distributions for the resonant electric dipole-ENG shell system obtained from the analytical model and the HFSS simulation model also showed very good agreement. The HFSS simulation results are shown in Fig. 9. It is apparent from Fig. 9 that the more realistic HFSS model provides a better insight into the behavior of the fields when a real radiating structure is present, e.g., the behavior of the E-field near the electric dipole antenna ends and gap. The noticeable large E-field spots seen across the DPS-ENG boundary are the numerical artifacts which, as discussed in the Appendix, are due to mesh resolution issues in that region of the ENG shell. Our numerical studies have shown that such hot spots had little effect on the RPR results given in Fig. 8 when the numerical model is well converged.

B. Electric Dipole-ENG Shell System Using a Lumped Element Model at 300 MHz

Having validated the HFSS models of the constant current source electric dipole antenna with and without the ENG shell, we generalized the model of the center-fed electric dipole antenna to one that is driven by an HFSS lumped element. The main advantage of using a lumped element over a current source element is that the former allows one to introduce a feed network into the model; and, as a result, it allows one to obtain the system's overall input impedance; its total radiated power for a specified input power; and, hence, its overall efficiency as functions of the driving frequency. To characterize the total radiated

power of the center-fed electric dipole-ENG shell system driven with a 1 W input power, we introduce the known relative gain (RG) parameter [18]

$$\mathrm{RG} = 10\log_{10}\left[\frac{\mathrm{P}_{\text{with shell}}(1\text{ W input})}{\mathrm{P}_{\text{without shell}}(1\text{ W input})}\right](\mathrm{dB}). \quad (6)$$

A z-oriented 300 MHz thin cylindrical electric dipole antenna of length $\ell = 10$ mm that had a lumped element feed was first modeled in free space to validate this HFSS model. The electric dipole was again defined using two identical PEC cylinders that were separated by a vacuum gap of length 0.2 mm. However, to obtain faster and more convergent simulation results, we increased the electric dipole's radius from 0.06 mm to 0.1 mm. Thus the radius of the cylindrical elecrtric dipole antenna was $r_{\text{antenna}} = 0.1\text{ mm} = \lambda_0/1000$ so that the aspect ratio $\ell/(2r_{\text{antenna}}) = 50.0$. The resistance and reactance values of the lumped element source were set to 50 Ω and 0 Ω, respectively. The input power from the source was taken to be 1 Watt. The computed radiation resistance and reactance values for the free-space electric dipole antenna driven at 300 MHz were, respectively, 10.26% and 6.32% different from the values obtained with the relations given in Balanis [18, pp. 566–570] for the approximate analytical input impedance: $Z_{\text{in}} = 0.01974 - \text{j}11119\ \Omega$. Further studies of the behavior of the radiation resistance and reactance as a function of frequency exhibited the behaviors expected from those analytical models.

This validated HFSS lumped element center-fed electric dipole model was then surrounded with the same frequency independent ENG shell system having $(\varepsilon, \mu) = (-3\varepsilon_0, +\mu_0)$ and $r_1 = 10$ mm. The HFSS predicted radiated power of the lumped-source center-fed electric dipole in the presence of the ENG shell normalized by its free space value is shown in Fig. 10. The maximum of this HFSS predicted relative gain was 64.05 dB at the outer radius $r_{2,\max} = 18.45$ mm. This RG result is in very good agreement with the analytical and the constant current source RPR results. A comparison of Figs. 8 and 10 clearly shows how the size of the antenna radius affected the behavior of the electric dipole-ENG shell system. The current source design results in Fig. 8 were obtained using a 0.06 mm radius electric dipole that is thinner than the 0.1 mm radius lumped element source electric dipole used to generate the results in Fig. 10. The effective capacitance of the former is greater than the latter. Consequently, the center-fed lumped element electric dipole-ENG shell system requires less inductance to compensate for this increased capacitive reactance and, thus, to maintain the resonant frequency. The resonant outer shell radius, therefore, is greater in Fig. 10 than it is in Fig. 8. We note that the relative gain is now a true gain quantity because the power input in both the electric dipole-free space and electric dipole-ENG shell cases was 1 Watt. We also note that while this seems to be an extraordinarily large gain, the free space electric dipole attached to the 50 Ω transmission line radiates only 1.636×10^{-8} W. Consequently, with no attempt to match it to the 50 Ω transmission line, the electric dipole-ENG shell system radiates 0.0416 W, giving an overall efficiency equal to 4.16%.

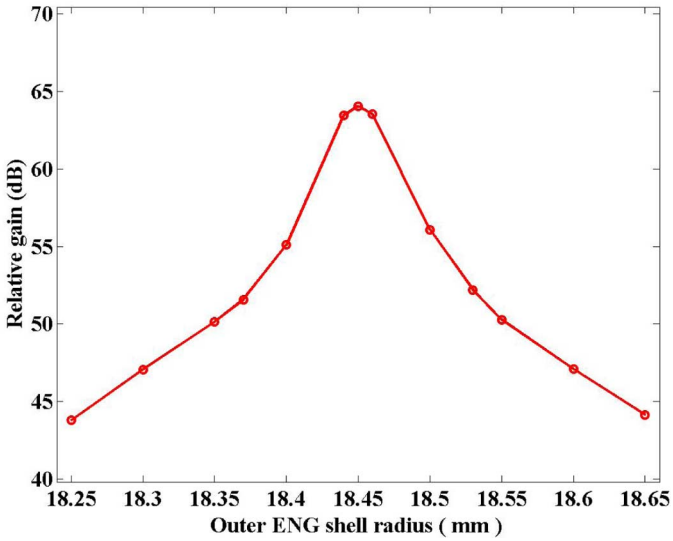

Fig. 10. The power radiated by the HFSS lumped element center-fed electric dipole model at 300 MHz enclosed in an ENG shell with a frequency independent relative permittivity $\varepsilon_r = -3.0$ and an inner radius $r_1 = 10.0$ mm normalized by the values for the same electric dipole radiating in free space, both having a 1 W input power. The maximum relative gain occurs at $r_{2,\max} = 18.45$ mm.

The input impedance of the center-fed electric dipole-ENG shell system with the present antenna dimensions was found to have a resonance $(X_{\text{in}} = 0)$ with the real input impedance $Z_{\text{in}} = 2479\ \Omega$ at 300 MHz. It also has an anti-resonance $(X_{\text{in}} = 0)$ with an input impedance $Z_{\text{in}} = 45,377\ \Omega$ at 341 MHz. Thus, with the present antenna and shell dimensions, the ENG shell simply produces a complex conjugate reactance match to the center-fed electric dipole, but it does not produce a 50 Ω match. While the radiation resistance at the resonance is high, we can now change the dimensions of the antenna and the ENG shell to achieve a complete match to the feedline. We note that, in contrast, the radiation resistance of the anti-resonance is indeed very large and would be difficult to match to the feedline. Nonetheless, these results clearly demonstrate, as anticipated, that this system is indeed resonant in the antenna-sense that the input reactance becomes zero indicating a balance between the capacitive nature of the electrically small electric dipole antenna and the inductive ENG shell.

With further modifications of the antenna and shell dimensions, a resonant center-fed electric dipole-ENG shell system that produced approximately a 50 Ω resistance and zero reactance near 300 MHz was designed. In particular, the system parameters were adjusted to reduce the moderately large radiation resistance value to 50 Ω by shifting the peak of the resistance curve to a frequency further above 300 MHz while maintaining the zero of the reactance curve at 300 MHz. Because the imaginary part of the complex valued impedance strictly depends on the system's capacitance, i.e., on the antenna's length and radius, it can be adjusted to pass through zero at the driving frequency by adjusting the antenna's radius size and/or the length of the electric dipole antenna. We note, however, that changing the antenna's length and radius, as well as the thickness of the ENG shell, have different but related impacts on the results. Some of these parameter variations are characterized below.

TABLE I
DETAILED SPECIFICATIONS OF THE MATCHED RESONANT ELECTRIC DIPOLE-ENG SHELL SYSTEM

Antenna Length	10 mm
Antenna Radius	2.5 mm
Gap Length	0.2 mm
Gap Radius	2.5 mm
Operation Frequency	300 MHz
Lumped Port Resistance Value	50 Ohm
Lumped Port Reactance Value	0 Ohm
Inner Shell Radius (r1)	10 mm
Outer Shell Radius (r2)	19.51mm

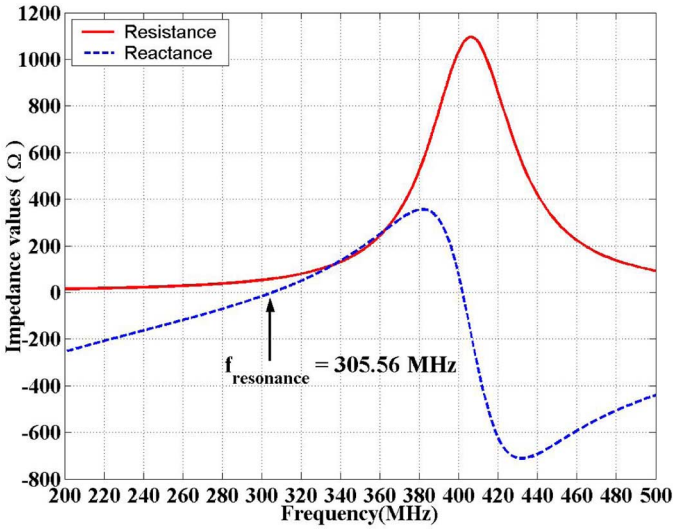

Fig. 11. The complex valued radiation impedance of the matched resonant electric dipole-dispersionless ENG shell system design. It is matched at 305.56 MHz to a feedline with 50 Ω resistance and zero reactance.

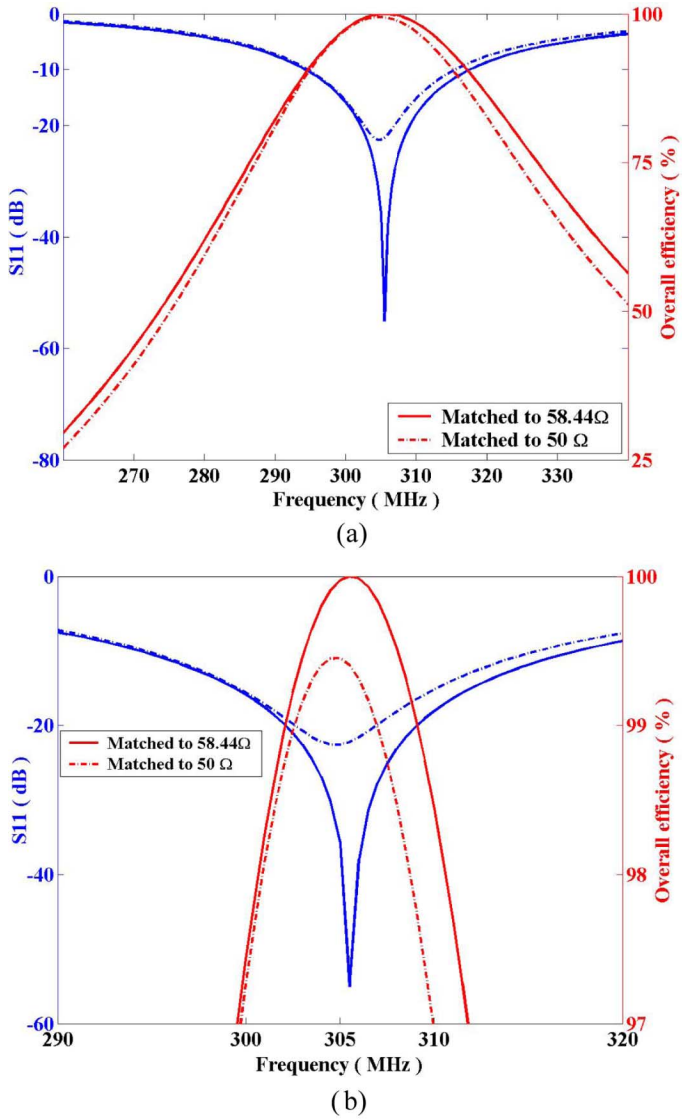

Fig. 12. S_{11} and overall efficiency values versus frequency for the resonant electric dipole-dispersionless ENG shell system design. The curves for matching the electric dipole-dispersionless ENG shell system to 50 Ω and a 58.44 Ω resistance sources are given. (a) S_{11} and overall efficiency vaues; (b) zoom.

Thus there are many different combinations that produce the same input impedance response. The detailed specifications of the HFSS model that we designed to be matched to the 50 Ω feedline are summarized in Table I. The radius of the wire was increased to 2.5 mm; the outer radius of the ENG shell that produced the resonant configuration was 19.51 mm. Fig. 11 shows the HFSS predicted values of the resistance and reactance for this design as a function of the frequency. The (resonance) zero crossing of the reactance occurs at 305.56 MHz and the resistance value at this frequency is 58.44 Ω. The resistance and reactance values at 300 MHz were 52.54 Ω and −17.00 Ω, respectively. The overall efficiency of this system for a 50 Ω source at 300 MHz was found to be 97.18%.

The S_{11} reflection coefficient values of this lumped element center-fed electric dipole-ENG shell system matched to the original 50 Ω source and to a 58.44 Ω matched network source are plotted in Fig. 12 to illustrate the potential overall efficiency of the overall system as a function of the frequency. These S_{11} parameter values were generated using the impedance values given in Fig. 11. First, a third order polynomial fit was applied to those discrete impedance values for the frequency region between 260 and 340 MHz. The third order polynomial coefficients were then used to define continuous curves that allowed us to plot the S_{11} parameters with a finer frequency resolution and, hence, determine straightforwardly the −10 dB frequency values for the bandwidth calculation. The polynomial coefficients were also used to calculate the derivatives of the resistance and reactance values at the frequency zero crossing point. The corresponding overall efficiency curves are also included in Fig. 12. They were obtained from the HFSS radiated power calculations $\mathrm{RE} = (P_{\mathrm{rad}}/P_{\mathrm{in}}) \times 100\%$ at the discrete frequency points and independently from calculations of the reflection coefficients $\mathrm{RE} = (1 - |S_{11}|^2) * 100\%$ from the polynomial fit; both were shown to be in excellent agreement for this matched, resonant system. The −10 dB frequency points of S_{11} in Fig. 12 are 294.3 and 317.48 MHz, respectively, for the 50 Ω match. Consequently, for this dispersionless-ENG-shell-based system the bandwidth with these transmission line matching values was $\mathrm{FBW_{TL}} = 7.73\%$, and the corresponding quality factor was $Q_{\mathrm{TL}} = 12.94$. The

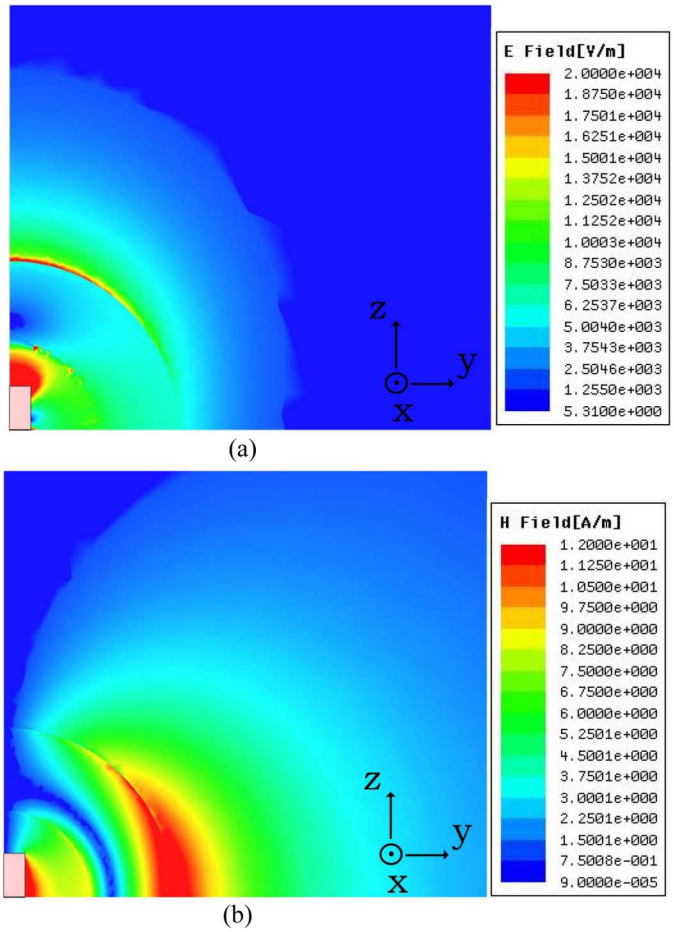

Fig. 13. E-field (a) and H-field (b) distribution plots (in one quadrant) for the resonant lumped element z-oriented center-fed electric dipole-dispersionless ENG shell system matched to the feedline at 305.5 MHz.

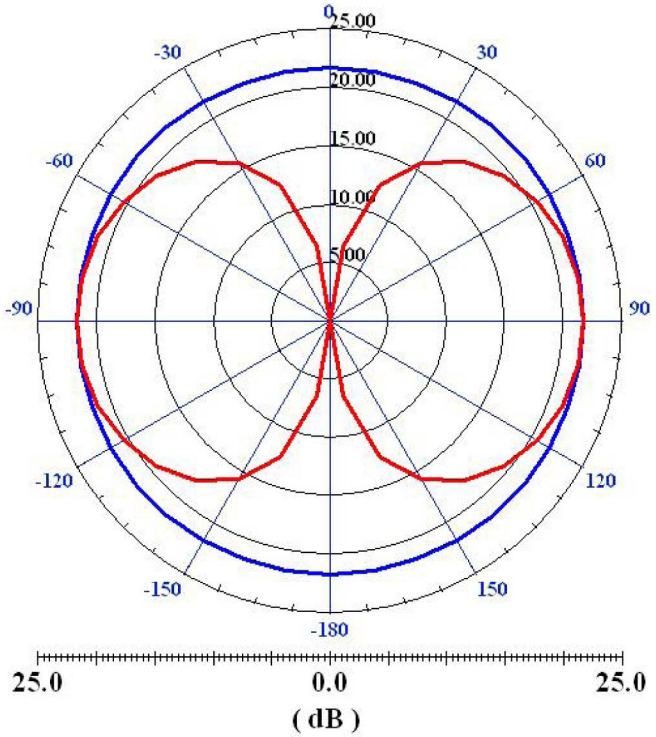

Fig. 14. HFSS predicted E- and H-plane patterns in the far-field region for the resonant lumped element z-oriented center-fed electric dipole-dispersionless ENG shell system matched to the feedline at 305.5 MHz. The E-plane (H-plane) pattern is the red (blue) curve.

-3 dB frequency points of the overall efficiency (50% values) for the 50 Ω match in Fig. 12 are 273.66 and 344.62 MHz. Consequently, the so-called fractional half-power VSWR bandwidth [16] was $\mathrm{FBW}_{\mathrm{VSWR,Dipole\ system}} = 23.65\%$ and the corresponding quality factor, using Yaghjian and Best's formula for Q [16, Eq. 87], $Q_{\mathrm{VSWR}}(\omega_0) = 2/\mathrm{FBW}_{\mathrm{VSWR}}(\omega_0)$ was $Q_{\mathrm{VSWR,Dipole\ system}} = 8.46$. The derivative values were used to calculate Yaghjian and Best's formula for Q [18, Eq. 86], written here for ease of computation with the given data in Fig. 11 as $Q_{\mathrm{YB}} \approx f_0|\partial_f Z_{\mathrm{input}}(f_0)|/2R(f_0)$. This value $Q_{YB} \approx 8.78$ gives the so-called fractional conductance bandwidth $\mathrm{FBW}_{\mathrm{CD}} = 1/\mathrm{Q}_{\mathrm{YB}} = 11.38\%$, which, as pointed out by [16, Eq. 42], is approximately half of the half-power VSWR FBW value reported above. We note that all of these Q and FBW values are in very good agreement. We also note that all of these Q values for this dispersionless ENG shell-based system are much smaller than the corresponding Chu limiting value: $k_0 r_e \equiv k_0 r_2 = 0.123$, $Q_{\mathrm{Chu\ limit}} = 545.39$. We further note that the FBW obtained from the RPR values for the analytical infinitesimal dipole-ENG shell system corresponds reasonably well to the fractional conductance bandwidth value. It slightly underestimates the FBW; hence, overestimates the Q value. This fact allows us to use with some assurance as to their accuracy, the analytically predicted infinitesimal electric dipole bandwidth results to discuss the dispersion effects below.

Fig. 13(a) and (b) show, respectively, plots of the HFSS predicted E-and H-field distributions. Fig. 14 shows the HFSS predicted E- and H-plane patterns in the far-field region for the resonant electric dipole-ENG shell system design that produced the 58.44 Ω resistance and zero reactance at 305.5 MHz. The radiation patterns for both cases agree with the well known electric dipole antenna radiation patterns confirming there is no variation in the pattern, hence the directivity, when the resonance occurs although there is an enhancement of the overall efficiency due to the presence of the matched dispersionless ENG shell.

In the design of the matched resonant center-fed lumped element electric dipole-dispersionless ENG system, we considered a number of variations in the parameters. Some of the results of this parameter study are summarized in Tables II and III. In Table II the radius of the electric dipole was varied while keeping its length and the ENG shell size constant. The resonant frequency of the system, i.e., the frequency at which the system's reactance passes through zero with a positive slope with respect to the frequency, was determined. For a fixed shell thickness and permittivity this resonant frequency decreases as the dipole's radius increases. On the other hand, the peak of the resistance curve increases as the dipole's radius increases. One can thus visualize this as the resistance curve is translated vertically as the dipole's radius increases. In Table III the length of the electric dipole is varied for a fixed shell size and radius of the dipole. The maximum resistance and reactance values increase when the dipole length increases. The results included in

TABLE II
THE MAXIMUM RESISTANCE VALUES, THE REACTANCE ZERO CROSSING FREQUENCIES, AND THE RESISTANCE VALUE AT THE RESONANT FREQUENCY FOR DIFFERENT ELECTRIC DIPOLE RADIUS SIZES USING A 2 mm INITIAL MESH VALUE ON THE SHELL SURFACE AT $r_2 = 18.45$ mm

Radius of the electric dipole (mm)	Maximum resistance value (Ω)	Reactance zero crossing frequency (MHz)	Resistance at resonant frequency (Ω)
0.01	36922	-	-
0.10	49698	293.68	4800
0.15	51165	259.50	3072
0.20	56196	253.00	2405

TABLE III
THE MAXIMUM VALUES OF THE RESISTANCE AND REACTANCE USING DIFFERENT ELECTRIC DIPOLE LENGTHS USING A 2 mm INITIAL MESH VALUE ON THE SHELL SURFACE AT $r_2 = 18.45$ mm WITH THE FIXED RADIUS OF THE ANTENNA BEING 1 mm

Half-length of the electric dipole (mm)	Maximum resistance value (Ω)	Maximum reactance value (Ω)
4.70	1399	-10750
4.80	3748	-3109
4.90	4005	-2873
5.00	5091	355

Table III indicate that large variations in the reactance values can occur for small variations in the dipole's length. On the other hand, the resistance values change relatively slowly in comparison. These observations were crucial to the design of the matched resonant configurations, particularly for those cases for which the reactance values were large but much smaller resistance variations were needed. In other words, if the resistance part is matched to a feed line but the reactance portion has a value largely different from zero, we found it a good practice to modify the antenna length instead of changing the other electric dipole-ENG shell system parameters to achieve a matched, resonant system. As shown in Fig. 8, the resonant outer radius size is smaller than the corresponding outer radius size in Fig. 10 to compensate for this additional capacitance.

IV. ELECTRICALLY SMALL COAX-FED MONOPOLE ANTENNA SURROUNDED BY AN ENG SHELL: HFSS RESULTS

While the lumped element center-fed electric dipole-ENG shell system results confirmed that the ENG shell can be matched to an electric dipole antenna to obtain a resonant system with interesting bandwidth properties, the lumped element model itself would require several components to be realized physically. The electromagnetic properties of those components would have to be considered in the final design of any prototype system fielded for experimental validation of these results as they could alter the specifications of the antenna

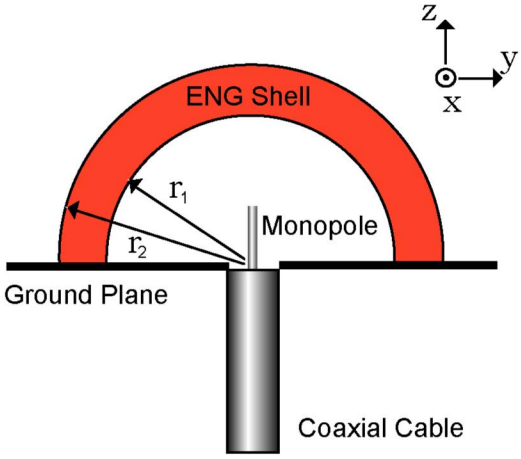

Fig. 15. HFSS model of the coax-fed monopole-ENG shell system.

or the ENG shell. On the other hand, a common approach used to realize an electric dipole antenna is to consider the corresponding monopole antenna over a ground plane. One of the simplest versions of this monopole antenna system is achieved by using a coaxial transmission line and a PEC ground plane.

As described in the Appendix, an HFSS model of a coaxially fed monopole antenna in which the center conductor of the coax protrudes through an infinite ground plane into free space was designed. The coaxial cable was defined below the xy plane; the monopole extended from the origin of the coordinate system into the $z > 0$ half space. The radius of the cylindrical center conductor of the coax r_a and, hence, the monopole antenna was $r_a = r_{\text{monopole}} = 0.1$ mm. The radius of the outer conductor r_b was set equal to $r_b = 2.301 r_a$ in order that the characteristic impedance of the coax TEM mode was $Z_0 = 60 \ln(r_b/r_a) = 50\ \Omega$. The TEM mode was driven at 300 MHz with a HFSS wave-port source that produced 1 Watt of input power. The length of the extension of the center conductor beyond the ground plane into free space was $\ell = 5$ mm and was taken along the positive z-axis. This monopole model allowed us to make comparisons with known approximate analytical results in Balanis [18, pp. 566–570]. The computed resistance and reactance values were, respectively, only 4.46% and 3.04% different from those analytical results, thus validating this HFSS monopole antenna model in free space. A sketch of the HFSS coax-fed monopole-ENG shell system model is shown in Fig. 15.

This validated HFSS coaxially-fed monopole antenna was then surrounded with the same frequency independent ENG shell system with $(\varepsilon, \mu) = (-3\varepsilon_0, +\mu_0)$ and $r_1 = 10$ mm that was discussed in Sections II and III. The HFSS predicted radiated power for the coaxially-fed monopole in the presence of the ENG shell normalized by its free space value is shown in Fig. 16. Relative gain results are in very good agreement with the analytical and the HFSS constant current and lumped element electric dipole-ENG shell system results. For example, the HFSS predicted maximum relative gain was 63.81 dB at the outer radius $r_{2,\max} = 18.45$ mm, which is only 0.3% different from what was predicted for the corresponding lumped element center-fed electric dipole-dispersionless ENG shell system.

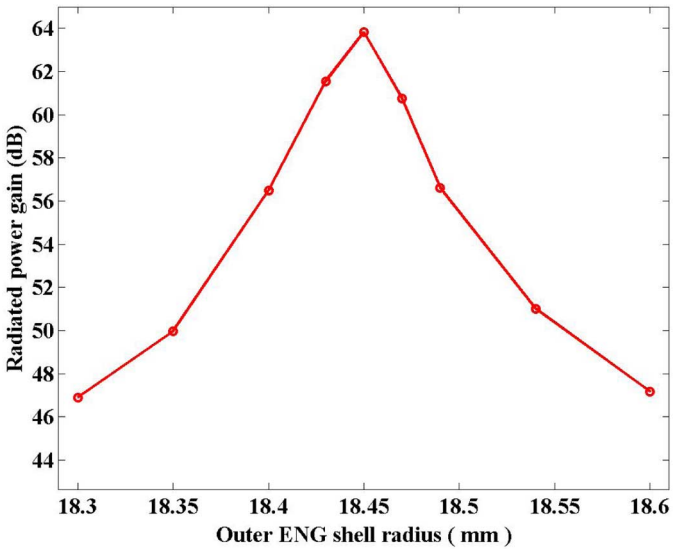

Fig. 16. The power radiated at 300 MHz by the coaxially-fed monopole antenna enclosed in an ENG shell with a frequency independent relative permittivity $\varepsilon_r = -3.0$ and an inner radius $r_1 = 10.0\,\mathrm{mm}$ normalized by the values for the same monopole radiating in free space. The maximum relative gain 63.81 dB occurs at $r_{2,\max} = 18.45\,\mathrm{mm}$.

The corresponding input impedance values of the coaxially-fed monopole antenna that is enclosed within an ENG shell system with a frequency independent relative permittivity $\varepsilon_r = -3.0$ and inner radius $r_1 = 10.0\,\mathrm{mm}$ had resonance and anti-resonance values as expected. The approximate location of the resonance obtained from the polynomial fit computations occurred at $r_2 = 18.44\,\mathrm{mm}$ with $Z_{\mathrm{in}} = 2083\,\Omega$. A comparison of the resonant outer radius values that were obtained from the HFSS lumped element center-fed electric dipole and coaxially-fed monopole antenna-ENG shell systems showed excellent agreement. The outer radius values for the resonance points found in these two cases differed by only 0.0065%. Moreover, a comparison of the resistance values at the anti-resonance and resonance points reveals an interesting characteristic of the proposed systems. Using a monopole rather than an electric dipole antenna reduced the resistance of the anti-resonance point from 45,377 Ω to 12,667 Ω. The 3.58-fold decrease in the maximum resistance value is in reasonable agreement with the small antenna formula in Balanis [18, pp. 566–570], where reducing the antenna size by half decreases the resistance value by 4. On the other hand, the corresponding resistance value at the resonance point was only slightly reduced from 2479 Ω to 2083 Ω. This property of the dispersionless ENG shell system was expected because the relative gain of these two systems was almost the same.

We note that the values of the total power radiated by the coaxially-fed monopole without and with the dispersionless ENG shell were, respectively, 6.8778×10^{-8} W and 0.0914 W. Since both the monopole without and with the dispersionless ENG shell have the same 1 Watt input power, the relative gain at resonance is again a true gain quantity. The S_{11} parameter value for the input impedance resonance was still significantly large, -0.4163 dB, due to the large mismatch between the characteristic impedance of the HFSS coaxial line, which was evaluated to be $Z_{\mathrm{in,coax}} = 49.913\,\Omega$, and the resonant input impedance value of the coaxially-fed monopole-dispersionless ENG shell system, $Z_{\mathrm{in}} = 2083\,\Omega$. The overall efficiency of this coaxially-fed monopole-dispersionless ENG shell system was thus 9.14%, in agreement with the RG result.

TABLE IV
DETAILED SPECIFICATIONS OF THE MATCHED RESONANT COAXIALLY-FED MONOPOLE-ENG SHELL SYSTEM

Monopole Antenna Length	4.65 mm
Monopole Antenna Radius	2.0 mm
Coaxial Inner Cylinder Radius	2.0 mm
Coaxial Outer Cylinder Radius	4.602 mm
Coaxial Transmission Line Length	52.04 mm
Operation Frequency	300 MHz
Coaxial Characteristic Impedance Value	49.913Ω Ohm
Inner Shell Radius (r1)	10 mm
Outer Shell Radius (r2)	19.06mm

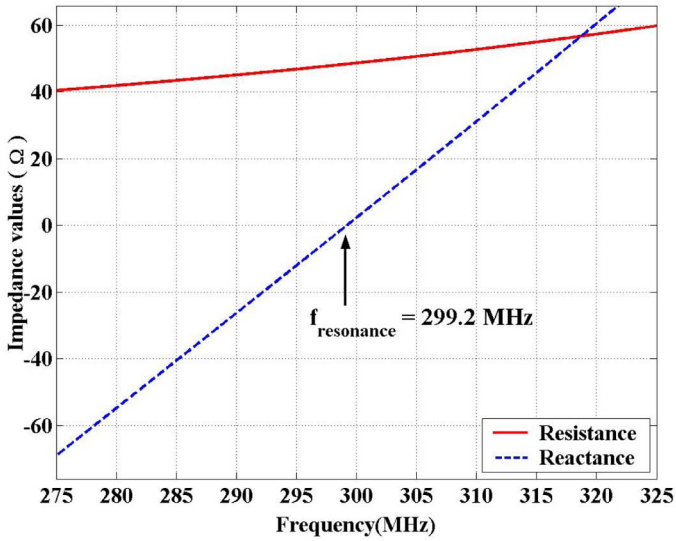

Fig. 17. The complex valued radiation impedance of the resonant coaxially-fed monopole-dispersionless ENG shell system design that is matched to a 50 Ω resistance and zero reactance near 300 MHz.

However, as shown for the HFSS lumped element center-fed electric dipole-dispersionless ENG shell system, the overall efficiency can be improved by further optimizing the system parameters to achieve an input impedance resonance that produces the value $Z_{\mathrm{in}} = 49.913\,\Omega$. The same brute-force optimization method that was used to improve the match to a 50 Ω source and, hence, the overall efficiency of the lumped element center-fed electric dipole-dispersionless ENG shell system was also applied to this coaxially-fed monopole-dispersionless ENG shell system. The detailed specifications of the optimized HFSS model of the resonant coaxially-fed monopole-dispersionless ENG shell system that matched the resistance of the coax feed and has zero reactance near 300 MHz is summarized in Table IV. A slightly smaller center conductor length (monopole length being 4.65 mm), center conductor radius (2.0 mm) and outer shell radius (19.06 mm) produced the desired matched, resonant system. Fig. 17 shows the HFSS predicted values of the resistance and reactance for this design as a function of the frequency. The zero crossing of the reactance values occurred

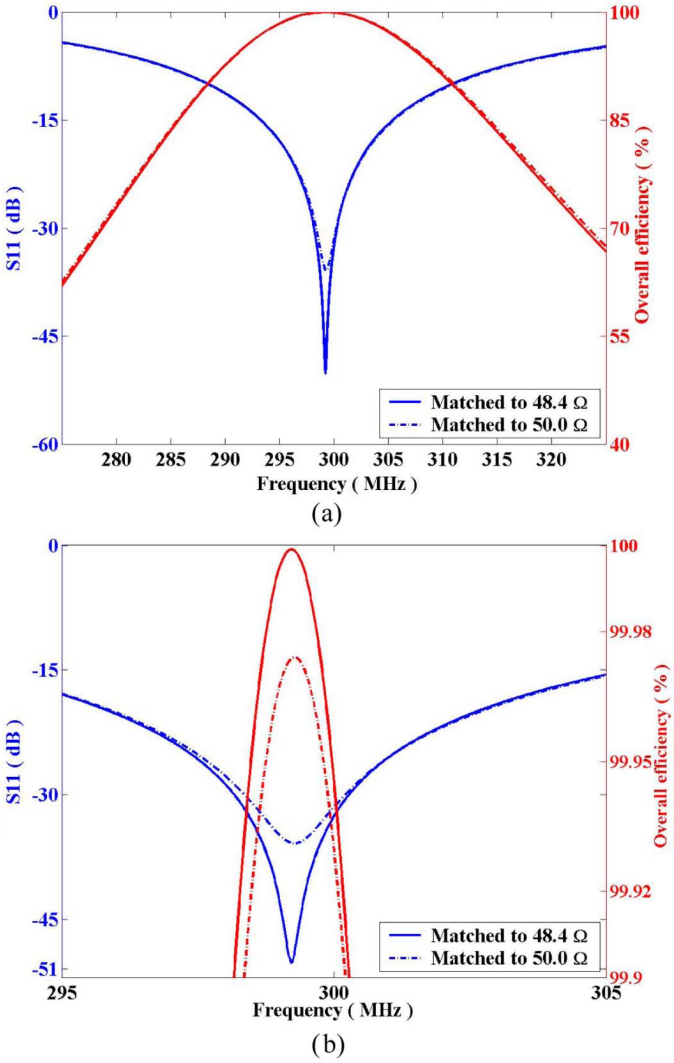

Fig. 18. The S_{11} and overall efficiency values versus frequency for the resonant coaxially-fed monopole-dispersionless ENG shell system design. The curves for matching the coaxially-fed monopole-dispersionless ENG shell system to 50 Ω and 48.40 Ω resistance sources are given. (a) S_{11} and overall efficiency values; (b) zoom.

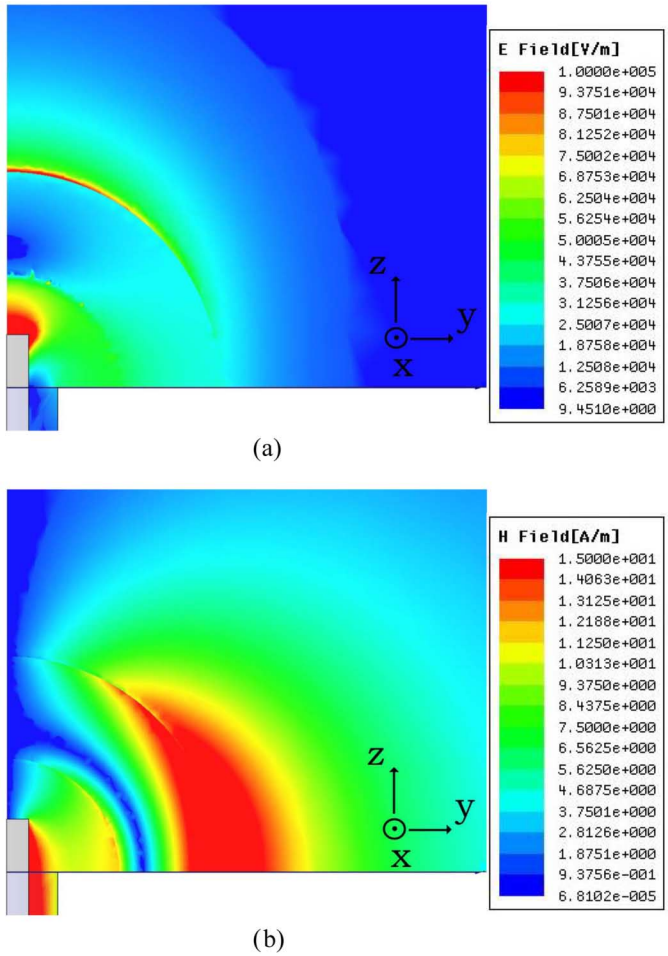

Fig. 19. E-field (a) and H-field (b) distribution plots (in one elevation plane) of the resonant coax-fed z-oriented monopole-dispersionless ENG shell system design that is matched to a 48.40 Ω resistance and zero reactance at 300 MHz.

at 299.212 MHz and the resistance and overall efficiency values at this frequency were 48.40 Ω and 99.999%, respectively. The overall efficiency of this system for a 50 Ω source at 300 MHz was 99.9285%.

The HFSS predicted S_{11} reflection coefficient values for this coaxially-fed monopole-dispersionless ENG shell system driven by the original 50 Ω source and by a 48.40 Ω matched network source are plotted in Fig. 18 to illustrate the overall efficiency of the system as a function of the frequency. These S_{11} parameter values were generated using the impedance values given in Fig. 17. First, a third order polynomial fit was applied to those discrete impedance values for the frequency region between 275 and 325 MHz. The third order polynomial coefficients were then used to define continuous curves that allowed us to plot the S_{11} parameters with a finer frequency resolution and, hence, determine straightforwardly the -10 dB frequency values for the bandwidth calculation. The polynomial coefficients were also used to calculate the derivatives of the resistance and reactance values at the resonance frequency. The corresponding overall efficiency curves are also included in Fig. 18. The -10 dB frequency points of S_{11} in Fig. 18 are 288.44 and 310.84 MHz, respectively. The -3 dB frequency points of the relative gain in Fig. 18 are 268.72 and 337.73 MHz. Consequently, the transmission line matching bandwidth and Q values are $\mathrm{FBW_{TL}} = 7.47\%$ and $Q_{\mathrm{TL}} = 13.39$, respectively; and the fractional half-power VSWR bandwidth and Q values are $\mathrm{FBW_{VSWR,Monopole\ system}} = 23.00\%$ and $Q_{\mathrm{VSWR,Monopole\ system}} = 8.70$, respectively. The derivative values obtained from Fig. 18 were again used to calculate Yaghjian and Best's formula for quality factor Eq. 86, [16]. The calculations yielded a value $Q_{\mathrm{YB}} \approx 8.95$, giving a fractional conductance bandwidth $\mathrm{FBW_{CD}} = 11.17\%$, which, as expected from [16, Eq. 42], is about a factor of two smaller than the fractional half-power VSWR bandwidth value. All of these quality factor values are in quite good agreement with the corresponding lumped element center-fed electric dipole-dispersionless ENG shell system results and are again much smaller than the corresponding Chu limiting value: $k_0 r_e \equiv k_0 r_2 = 0.1197$, $Q_{\mathrm{Chu\ limit}} = 590.45$.

Fig. 19(a) and (b) show, respectively, plots of the HFSS predicted E-and H-field distributions of the resonant coaxially-fed

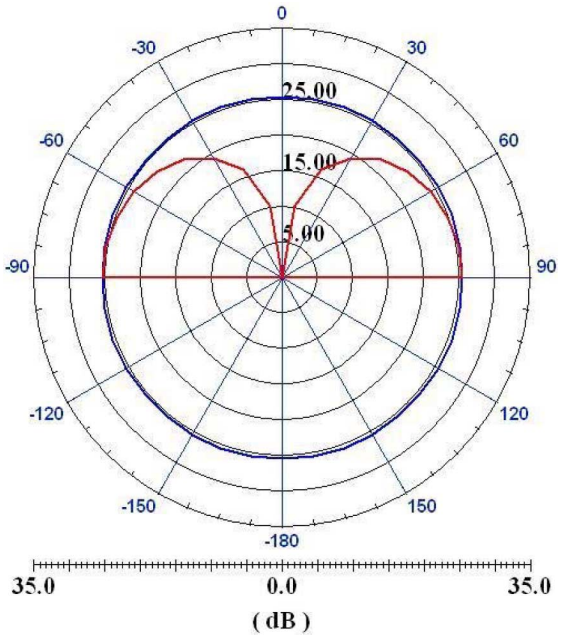

Fig. 20. The HFSS predicted E- and H-plane patterns in the far-field region for the resonant z-oriented coaxially-fed monopole-dispersionless ENG shell system design that produced a 48.40 Ω resistance and zero reactance at 300 MHz. The E-plane (H-plane) pattern is the red (blue) curve.

TABLE V
THE FRACTIONAL BANDWIDTH AND RESULTING DUALITY FACTORS FOR THE INFINITESIMAL ELECTRIC DIPOLE-LOSSY DRUDE ENG SHELL SYSTEMS

Γ/ω_0	Efficiency η_{rad}	RPR (dB)	FBW %	Q_{ratio}
0.0	1.0	63.218	0.1027	1.5833
1.0×10^{-5}	0.9905	63.178	0.1037	1.5831
1.0×10^{-4}	0.9123	62.821	0.1126	1.5835
1.0×10^{-3}	0.5098	60.294	0.2015	1.5832
1.0×10^{-2}	0.0942	50.961	1.0911	1.5826

monopole-dispersionless ENG shell system. The field distributions are slightly different than in the center-fed electric dipole case because of the differences in the antenna. The presence of the monopole and its feed line and the subsequent redistribution the resonant mode pattern are clearly seen. Fig. 20 shows the HFSS predicted E- and H-plane patterns in the far-field region for the resonant coax-fed monopole-dispersionless ENG shell system design that produced the 48.40 Ω resistance and zero reactance at 299.20 MHz. The radiation patterns for both cases agree with the well known monopole-over-ground-plane antenna radiation patterns confirming there is no variation in the pattern although there is a resonant overall efficiency enhancement due to the presence of the matched ENG shell.

V. ELECTRIC DIPOLE-ENG SHELL SYSTEM WITH DISPERSION

The infinitesimal and center-fed electric dipole-dispersionless ENG shell systems were demonstrated to have a radiation quality factor significantly lower than the Chu limit. Theoretically, this is a very surprising result and seemingly contradicts the conclusions in [16] and [40] concerning increasing the bandwidth of an antenna with metamaterials. It indicates that if one could achieve constant negative values of the permittivity over a substantial frequency range, one could indeed construct an

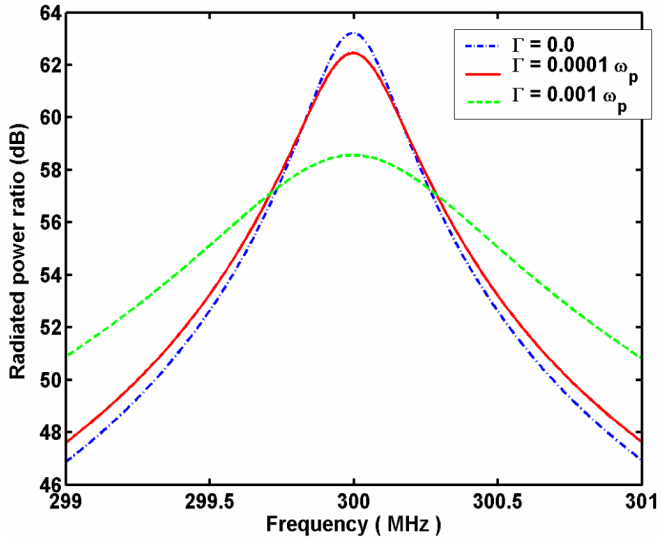

Fig. 21. Radiated power for a $\ell = 10$ mm infinitesimal dipole in lossless and lossy $r_1 = 10$ mm, $r_2 = 18.79$ mm Drude ENG shell with $\omega_p = 2\omega_0$ normalized by the power radiated by the same infinitesimal electric dipole in free space.

EESA that beats the Chu limit. Unfortunately, all negative permittivity metamaterials must exhibit dispersive properties [41]. The ones that have been created to date all exhibit at best a lossy Drude behavior, i.e.

$$\varepsilon_r(\omega) = \frac{\varepsilon(\omega)}{\varepsilon_0} = 1 - \frac{\omega_p^2}{\omega(\omega - j\Gamma)} = \left[1 - \frac{\omega_p^2}{\omega^2 + \Gamma^2}\right] - j\left[\frac{\Gamma\omega_p^2}{\omega(\omega^2 + \Gamma^2)}\right] \tag{7}$$

where ω_p is the plasma frequency and Γ is the collision frequency of the Drude model. The Drude medium exhibits ENG behavior for all angular frequencies $\omega < \sqrt{\omega_p^2 - \Gamma^2}$. It is lossless when $\Gamma = 0$; and in that case, the permittivity crosses zero at the angular frequency $\omega = \omega_p$. This Drude model is readily incorporated into the infinitesimal electric dipole-ENG shell analysis, and the RPR can be obtained as a function of the frequency.

The RPR results for the Drude ENG shell with $r_1 = 10$ mm and $r_2 = 18.79$ mm, were obtained for $\text{Re}[\varepsilon_r(\omega_0)] = -3.0$, i.e., for $\omega_p = 2\sqrt{\omega_0^2 + \Gamma^2}$, when $\Gamma/\omega_p = 0.0, 0.00001, 0.0001, 0.001$, and 0.01. The peak values of the RPR and fractional bandwidths for these cases were obtained and are summarized in Table V. The RPR results as functions of the frequency, when $\Gamma/\omega_p = 0$, 0.0001, and 0.001, are shown explicitly in Fig. 21. This figure shows that the shell size determined from the outer radius scans holding the inner radius, the permittivity, and the frequency fixed, provides the configuration that produces a resonant peak result at that frequency even when the ENG medium is dispersive and lossy. Moreover, because of the presence of the loss, it shows that there is a decrease in that peak value and, hence, the radiation efficiency of the system.

To obtain the quality factor when losses are present, the efficiency of the radiation process was calculated by taking the ratio of the total radiated power measured at $r_2 + \Delta$ (just outside the

ENG shell) to that measured at $r_1 - \Delta$ (just inside the ENG shell). This radiation efficiency, $\eta_{\rm rad}$, was calculated for each of the Drude model cases; these values are also given in Table V. We further note that when the radiation process is lossy, the expression for the quality factor in the Chu limit must be modified to: $Q_{\rm Loss,Chu} = \eta_{\rm rad} Q_{\rm Chu}$. To compare the quality factor obtained from the FBW to the Chu limt value when losses may be present in the ENG shell, we introduce the ratio

$$Q_{\rm ratio} = \frac{Q_{\rm BW,Lossy\ Drude}}{Q_{\rm Loss,Chu}} = \frac{1}{{\rm FBW}_{\rm BW,Lossy\ Drude}} \frac{1}{\eta_{\rm rad} Q_{\rm Chu}} \tag{8}$$

If this quality factor ratio is less (greater) than one, the Q of the system is smaller (greater) than the Chu limit value.

Combining the fractional bandwidths and the radiation efficiencies obtained for each of the Drude cases considered, the quality factor ratio for these infinitesimal electric dipole-lossy Drude ENG shell systems was determined. They are also given in Table V. From Table V we find, as was expected, that the FBW increases as the amount of loss is increased. Nevertheless, the value of the quality factor in the presence of loss remains essentially the same as the lossless value, i.e., $Q_{\rm ratio} \approx 1.583$, for all of the cases considered. This result indicates that it is sufficient to consider the lossless dispersion model to understand the FBW and quality factor behaviors. We thus conclude that when an ENG Drude shell is used, whether it is lossless or lossy, the quality factor of this system is slightly above the Chu limit.

On the other hand, since the Q values of these Drude-shell-based systems are near the Chu limit, we must ask whether or not there is a dispersive ENG medium which will lead to a FBW that comes closer to the idealized dispersionless values and, hence, to Q values below the Chu limit. To obtain a partial answer to this question, the Landau-Lifschitz (LL) limiting behavior for dispersion: $\partial_\omega(\omega\varepsilon_r) \geq 1$ [42], which corresponds to the limits discussed in [16, Eq. (70b)], was considered. A lossless ENG medium that exhibits this LL limiting behavior was achieved by introducing the lossless linear dispersion model

$$\varepsilon(\omega) = \varepsilon_0 \left[4.01 \left(\frac{\omega - \omega_0}{\omega_0} \right) - 3 \right] \tag{9}$$

to describe the permittivity of the ENG shell. This frequency dependent model yields $\varepsilon_r(\omega_0) = -3$ and satisfies the LL criterion over the frequency band of interest. Calculating the RPR values for this system, it was found that the peak value 63.22 dB occurs at $f_{0\ \rm dB} = 299.9939$ MHz and the half RPR values occur at the frequencies $f_{-3\ \rm dB} = 299.6895$ MHz and $f_{+3\ \rm dB} = 300.2985$ MHz, which means that the $FBW_{\rm LL\ disp} = 0.203\%$. Thus the lossless dispersion model yields a radiation quality factor for the resonant frequency that is slightly below the Chu limit: $Q_{\rm BW,LL\ disp} = 492.60 = 0.798\, Q_{\rm Chu\ limit}$, i.e., $Q_{\rm ratio} = 0.798$.

Finally, a direct comparison of the RPR curves for the lossless cases without dispersion, with the lossless linear dispersion LL limit model, with the lossy Drude dispersion model, and with the lossless Drude dispersion model for the same resonant infinitesimal electric dipole-ENG shell geometry are shown in Fig. 22 to extenuate these differences. Most importantly, it shows that the width of the frequency response has become much narrower in the presence of dispersion. Clearly, it also demonstrates that the peak RPR values for the lossless dispersion cases recover the dispersionless value at the resonance frequency. The narrower frequency dependence of the RPR when dispersion is present is to be expected because the resonant configuration is highly dependent on the value of the permittivity; and, consequently, the resonance is quickly detuned when the permittivity is varied with the frequency. We are currently investigating in more detail the theoretical limits on the FBW of these resonant configurations in relation to the Chu limit and will report these results elsewhere.

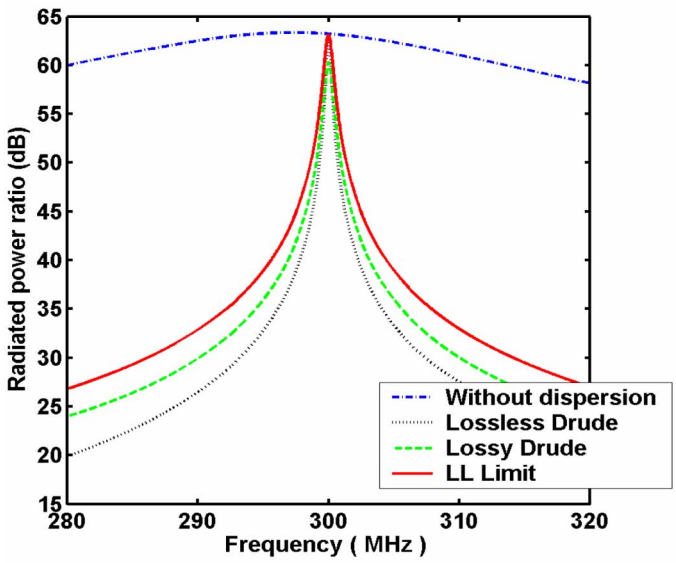

Fig. 22. Power radiated by a $\ell = 10$ mm infinitesimal electric dipole in a $r_1 = 10$ mm, $r_2 = 18.79$ mm ENG shell whose permittivity is described by several dispersion models normalized by the power radiated by the same infinitesimal electric dipole in free space.

In summary, the presence of dispersion and losses in the ENG shell causes the infinitesimal electric dipole-ENG shell system to have a frequency response that is much narrower than the one produced with the hypothetical constant negative permittivity value. Nonetheless, the results presented here show that the corresponding quality factors can still be near to or even potentially below the Chu limit if the dispersion properties of the ENG shell are properly engineered. In particular, because the main difference between the Drude and the LL models is the value of the rate of change of the permittivity through the resonance frequency, i.e., $\partial_\omega[\omega\varepsilon_{r,Drude}](\omega_0) = 5$ and $\partial_\omega[\omega\varepsilon_{r,LL}](\omega_0) = 1.01$, it is desirable to develop a low-loss dispersive ENG metamaterial that has the smallest possible variation in its permittivity values near the geometry resonance. Moreover, since we have shown above that the more detailed lumped element, center-fed electric dipole-ENG shell HFSS model yields slightly larger bandwidth values than those obtained with the corresponding infinitesimal electric dipole-ENG shell system, these results are encouraging and suggest that the

realistic metamaterial-based EESA's may also exhibit these very attractive bandwidth characteristics.

VI. Conclusion

Electrically small antenna systems formed by combining an infinitesimal electric dipole with an ENG spherical shell were considered analytically. It was demonstrated that such systems can be made to be resonant with a resulting very large enhancement of the radiated power in comparison to the antenna alone in free space. The inductive nature of the ENG shell was used to compensate for the capacitive nature of the electrically small electric dipole antenna to form this resonant system. Comparisons of the analytical ENG spherical shell systems were given. Losses and dispersion characteristics of the materials were included in these analytical models.

More realistic electrically small antenna systems formed by combining a center-fed cylindrical electric dipole and a coaxially-fed monopole over an infinite ground plane with an ENG spherical shell were then considered numerically. The finite element simulation tool, HFSS, was used to evaluate their performance. The development of the HFSS numerical models used for these evaluations was discussed. The input resistance and reactance of the realistic antenna-ENG shell systems were obtained from these numerical models and were shown to have antenna resonances where the corresponding relative gains and overall efficiencies were maxima. It was demonstrated that for all of the antennas considered with several variations in their sizes, an ENG shell could be designed to produce a resonant system. It was shown in particular that systems could be designed to have a zero input reactance and an input resistance that is matched to a specified source resistance to yield a very high overall efficiency. These systems were evaluated assuming ideal frequency independent ENG material properties; they were shown to be efficient and to have bandwidths and quality factors below the Chu limit without any degradation in the radiation patterns of the constituent antenna.

Having determined that a properly designed ENG shell provides a distributed matching element to an infinitesimal electrically small electric dipole antenna, one could ask why one should bother with the shell rather than simply immersing the electric dipole directly into an ENG sphere. An ENG sphere configuration is obtained by setting the material parameters, which are defined in Fig. 1, in Regions 2 and 3 to free space and in Region 1 to $\varepsilon_1 = \varepsilon_r - j\varepsilon_{im}$, $\mu_1 = \mu_0$. This configuration in the small sphere limit has been considered, for instance, in [43]. The coefficient of the source field for an infinitesimal electric dipole centered in an electrically small sphere is the same as the one for Rayleigh scattering from an electrically small sphere [44], i.e., in the limit that the radius goes to zero it is proportional to $1/(\varepsilon_r + 2)$ and thus the radiated field becomes singular for the lossless $\varepsilon_r = -2.0$ case. We have found that there are resonant electric dipole-sphere shell systems for permittivity values approaching this singular case. The use of such an ENG sphere to enhance the performance of an electrically small antenna was considered in [45]. Experimental results have been reported that show enhanced radiated power from an electrically small antenna that is completely surrounded by a plasma of finite size and is driven at frequencies below the plasma frequency [46]. We are currently investigating the various advantages and disadvantages of these ENG shell and solid sphere systems for our proof-of-concept experiments.

Using the analytical results, it was shown that the inclusion of material dispersion into the properties of the ENG shell has a significant impact on the bandwidth performance of the electric dipole-ENG shell systems, but not on their other performance characteristics such as the peak total radiated power or radiation patterns. It was demonstrated with the Drude model that introducing losses into the dispersive ENG shell increases the FBW and decreases the radiation efficiency, even though the overall quality factor remains the same—slightly above the Chu limit. With a dispersion model that satisfies an energy-based (Landau-Lifschitz) constraint, it was shown that the FBW can be below the corresponding Chu value. In constrast to the Drude model, this LL-based dispersion model of the permittivity was shown to have a much slower frequency variation at the resonance frequency of the electric dipole-ENG shell system. Clearly, trying to minimize the effects of the dispersion and losses of the ENG metamaterial on the overall system in the frequency band of interest would be a significant challenge, but a very worthy research direction. We are currently trying to develop an ENG metamaterial that has as many of these desirable attributes as possible for the spherical geometries considered here for proof-of-concept experimental validations of our results.

Appendix
HFSS Simulation Models

The constant current center-fed cylindrical electric dipole antenna was defined in HFSS using two identical perfect electric conductor (PEC) circular cylinders that were separated by a vacuum gap, another circular cylinder. The total length of the cylindrical antenna was $\ell = 10$ mm. The radius of the cylindrical antenna was $r_{\text{antenna}} = 0.06 \text{ mm} = \lambda_0/16666$; hence, the diameter of the gap was 0.12 mm. The length of the vacuum gap was 0.2 mm. The radii of the three cylinders were identical, and they were positioned symmetrically at the origin of the coordinate system and oriented along the z axis. This antenna was fed with an HFSS current source element; it was defined between the bottom and top faces of the vacuum cylinder. The magnitude of the current source was defined to be 1.0 A. This constant current source model is thus the same as the analytical model's source. The antenna was driven at 300 MHz, hence, $\ell/\lambda_0 = 0.01$. The radiation boundary was modeled using a cube that was centered at the xyz origin and had an edge length of 540 mm. The radiation boundaries were at least $\lambda_0/4$ from the radiating system in every direction. A PEC symmetry plane along the xy-plane and two perfect magnetic conductor (PMC) symmetry planes along the yz- and xz-planes were used to reduce the size of the computational space. The convergence of the simulation process was improved using initial meshing on the faces of the two PEC cylinders and on the inside of the vacuum gap. We used a 0.6 mm initial mesh on the dipole's surface and a 0.013 mm initial mesh in the vacuum gap. The lambda refinement value was set to 0.03 to promote finer meshing.

The HFSS model of the ENG shell was based upon a 60 segment polygonal approximation of the equator of the sphere. The E-field resolution across the DPS-ENG boundaries in the constant current center-fed cylindrical dipole antenna-ENG shell case was simulated by assigning an initial triangular mesh on the shell surface with a maximum edge length of 1 mm or less. Because of this fine initial mesh specification, each simulation required a tremendous amount of memory, about 7 GB of RAM. Consequently, we had to run these simulations on a UNIX operating system. The final mesh contained 148,297 tetrahedra; and for a 300 MHz λ-refinement frequency, there was a $\Delta E = 3.26$ variation in the E-field magnitude parameter. We found that the default value, which used a 20 segment approximation, did not produce consistent, convergent results. Hot spots appeared in certain mesh refinement zones that acted as reactive field regions and removed power from the radiated field. With sufficient refinement their impact on the results was significantly reduced However, with our current computer resources, we could not run any finer simulations for the resonance cases.

The center-fed electric dipole-ENG shell system at 300 MHz was then modeled using the HFSS lumped element. The lumped element allows one to introduce a feed network into the model in order to obtain the system's overall input impedance. Moreover, it allows one to run frequency sweeps for a given model. Because we expected to study a number of parameter variations with this model, we increased the dipole's radius from 0.06 mm to $r_{\text{antenna}} = 0.1 \text{ mm} = \lambda_0/1000$ to decrease the computational requirements of the model. Thus the aspect ratio was reduced to $\ell/(2r_{\text{antenna}}) = 50.0$. The length of the electric dipole and the gap size remained the same.

The lumped port of the source model was defined using a rectangle along the yz-plane between the bottom and top faces of the PEC cylinders. The radii of the two cylinders and the half-width of the rectangle along the y-axis were identical. The integration line of the lumped element source was defined along the z-axis from the center of the bottom PEC cylinder to the center of the top PEC cylinder. The resistance and reactance values of the lumped element source were set to 50 Ω and 0 Ω, respectively. The PEC cylinders were again positioned symmetrically about the origin of the coordinate system and oriented along the z-axis. The radiation boundary was again modeled using a cube with a 540 mm side length. A PEC symmetry plane along the xy-plane and two PMC symmetry planes along the yz- and xz-planes were used to reduce the computational space. The lambda refinement value was again set to 0.03 to promote finer meshing. The initial meshing on the polynomial shell surface was again set equal to 1 mm. The HFSS simulation required 153,143 tetrahedra and produced a variation in the S-parameters of $\Delta \text{S} = 0.0053$ for a 300 MHz λ-refinement frequency. The final convergence value was significantly better than the results obtained with the constant current source element because of the larger radius size for the electric dipole antenna.

Unfortunately, these HFSS simulations, while being very accurate, were still not suitable for optimizing the electric dipole-ENG shell system parameters due to their large memory requirements and associated long simulation times. We determined that the major reason for the large HFSS simulation space was due to the initial meshing on the polygonal-based spherical shell. Many HFSS simulations suggested that an initial meshing on the polygonal shell surface that was equal to or less than 1 mm produced convergent results for the current source model. The lumped element model was then designed with the same parameters to maintain the accuracy and also to provide one-to-one comparisons between the current and lumped element source model results. We decided to optimize the size of the initial meshing on the shell surface to reproduce the same impedance values as if it were run using the 1 mm initial meshing on the shell surface. A suite of HFSS simulation results suggested that a 2 mm initial meshing produced acceptable impedance values that were comparable with the 1 mm results. This reduced model was then used to design the resonant center-fed lumped element electric dipole-ENG shell system discussed in Section III that was matched to a 50 Ω source.

An HFSS model of a coaxially-fed monopole antenna in which the center conductor of the coax protrudes through an infinite ground plane into free space was designed. The coaxial cable was modeled using two concentric PEC cylinders. The monopole, an extension of the center conductor, was thus treated as a PEC cylinder. The coaxial cable was defined below the xy plane; the monopole extended from the origin of the coordinate system into the $z > 0$ half space. The HFSS source integration line was directed from the inside edge of the outer conductor of the coax to the outside edge of the inner conductor. The HFSS wave-port source was de-embedded to the origin to obtain the S_{11} coefficients simply by comparing monopole's impedance value and the coaxial cable's characteristic's impedance. In other words, we removed the extra reflection phase that would appear from the propagation of the wave along the coaxial transmission line. The radius of the cylindrical center conductor of the coax r_a and, hence, the monopole antenna was $r_a = r_{\text{monopole}} = 0.1 \text{ mm}$. The radius of the outer conductor r_b was set equal to $r_b = 2.301 r_a$ in order that the characteristic impedance of the coax TEM mode was $Z_0 = 60 \ln(r_b/r_a) = 50\,\Omega$. The TEM mode was driven at 300 MHz with a HFSS wave-port source that produced 1 Watt of input power. The length of the coaxial cable measured from the ground plane was set equal to $l_{\text{coax}} = 0.25\lambda_0$. The length of the extension of the center conductor beyond the ground plane into free space was $\ell = 5 \text{ mm}$ and was taken along the positive z-axis. This validated HFSS coaxially-fed monopole antenna was then surrounded with the same ENG shell system with $(\varepsilon, \mu) = (-3\varepsilon_0, +\mu_0)$. The HFSS simulation required 124,767 tetrahedra and produced a $\Delta \text{S} = 0.0135$ variation in the S-parameters for a 300 MHz λ-refinement frequency. The convergence and run times of the HFSS simulation process was again improved using the 0.2 mm initial meshing on the face of the monopole antenna. The radiation boundary was modeled using a rectangle that was centered at the origin and the xyz dimensions of the simulation space were set to $540 \text{ mm} \times 540 \text{ mm} \times 270 \text{ mm}$. These radiation boundaries were at least $\lambda_0/4$ from the radiating system in every direction. An infinitely large ground plane was defined along the xy-plane and two perfect magnetic conductor (PMC) symmetry planes along the yz- and xz-planes were used to reduce the computational space. The lambda refinement value

was set to 0.03 to promote finer meshing. The results were obtained again by using a 2 mm initial mesh on the ENG shell surface to minimize the size of the simulation space. A variety of comparisons with a 1 mm initial meshing again verified the validity of this approach.

ACKNOWLEDGMENT

The authors would like to thank several anonymous reviewers for their constructive comments which led to important additions and changes to this paper.

REFERENCES

[1] L. J. Chu, "Physical limitations of omnidirectional antennas," *J. Appl. Phys*, vol. 19, pp. 1163–1175, Dec. 1948.

[2] H. A. Wheeler, "Fundamental limitations of small antennas," *IRE Proc.*, vol. 35, pp. 1479–1484, Dec. 1947.

[3] ——, "The radiansphere around a small antenna," *IRE Proc.*, vol. 47, pp. 1325–1331, Aug. 1959.

[4] R. E. Collin and S. Rothschild, "Evaluation of antenna Q," *IEEE Trans. Antennas Propag.*, vol. AP-12, no. 1, pp. 23–27, Jan. 1964.

[5] R. L. Fante, "Quality factor of general ideal antennas," *IEEE Trans. Antennas Propag.*, vol. AP-17, no. 3, pp. 151–155, Mar. 1969.

[6] H. A. Wheeler, "Small antennas," *IEEE. Trans. Antennas Propag.*, vol. AP-23, Jul. 1975.

[7] E. H. Newman, P. Bohley, and C. H. Walter, "Two methods for the measurement of antenna efficiency," *IEEE Trans. Antennas Propag.*, vol. AP-23, no. 4, pp. 457–461, Jul. 1975.

[8] G. S. Smith, "Efficiency of electrically small antennas combined with matching networks," *IEEE Trans. Antennas Propag.*, vol. AP-40, no. 5, pp. 369–373, May 1977.

[9] R. C. Hansen, "Fundamental limitations in antennas," *Proc. IEEE*, vol. 69, pp. 170–181, Feb. 1981.

[10] L. Fante, "Maximum possible gain for an arbitrary ideal antenna with specified quality factor," *IEEE Trans. Antennas Propag.*, vol. AP-40, no. 12, pp. 1586–1588, Dec. 1992.

[11] J. S. McLean, "A re-examination of the fundamental limits on the radiation Q of electrically small antennas," *IEEE Trans. Antennas Propag.*, vol. AP-44, pp. 672–676, May 1996.

[12] S. R. Best, "The radiation properties of electrically small folded spherical helix antennas," *IEEE Trans. Antennas Propag.*, vol. 52, no. 4, pp. 953–960, Apr. 2004.

[13] ——, "A discussion on the properties of electrically small self-resonant wire antennas," *IEEE Antennas Propag. Mag.*, vol. 46, no. 6, pp. 9–22, Dec. 2004.

[14] ——, "A discussion on the quality factor of impedance matched electrically small wire antennas," *IEEE Trans. Antennas Propag.*, vol. 53, no. 1, pp. 502–508, Jan. 2005.

[15] ——, "Low Q electrically small linear and elliptical polarized spherical dipole antennas," *IEEE Trans. Antennas Propag.*, vol. 53, no. 3, pp. 1047–1053, Mar. 2005.

[16] A. D. Yaghjian and S. R. Best, "Impedance, bandwidth, and Q of antennas," *IEEE Trans. Antennas Propag.*, vol. 53, no. 4, pp. 1298–1324, Apr. 2005.

[17] R. P. Harrington, *Time Harmonic Electromagnetic Fields*. New York: McGraw-Hill, 1961, pp. 414–420.

[18] C. A. Balanis, *Antenna Theory*, 3rd ed. New York: Wiley, 2005, pp. 637–641.

[19] G. Skahill, R. M. Rudish, and J. Piero, "Electrically small, efficient, wide-band, low-noise antenna elements," in *Proc. Antenna Applications Symp.*, Allerton Park, Monticello, IL, Sep. 16–18, 1998, pp. 214–231.

[20] Y. Kim and D. L. Jaggard, "The fractal random array," *Proc. IEEE*, vol. 74, pp. 1278–1280, Sep. 1986.

[21] C. Puente, J. Romeu, and A. Cardama, "Fractal antennas," in *Frontiers in Electromagnetics*, D. H. Werner and R. Mittra, Eds. Piscataway, NJ: IEEE Press, 2000, pp. 48–93.

[22] D. H. Werner, R. L. Haupt, and P. L. Werner, "Fractal antenna engineering: the theory and design of fractal antenna arrays," *IEEE Antennas Propag. Mag.*, vol. 41, no. 5, pp. 37–59, Oct. 1999.

[23] D. H. Werner and S. Ganguly, "An overview of fractal antenna engineering research," *IEEE Antennas Propag. Mag.*, vol. 45, no. 1, pp. 38–56, Feb. 2003.

[24] K. J. Vinoy, K. A. Jose, V. K. Varadan, and V. V. Varadan, "Hilbert curve fractal antenna: a small resonant antenna for VHF/UHF applications," *Microw. Opt. Technical Lett.*, vol. 29, no. 4, pp. 215–219, May 2001.

[25] S. R. Best, "A comparison of the performance properties of the Hilbert curve fractal and meander line monopole antennas," *Microw. Opt. Technical Lett.*, vol. 35, no. 4, pp. 258–262, Nov. 2002.

[26] J. Zhu, A. Hoorfar, and N. Engheta, "Peano antennas," *IEEE Antennas Wireless Propag. Lett.*, vol. 3, pp. 71–74, 2004.

[27] ——, "Bandwidth, cross polarization, and feed-point characteristics of matched Hilbert antennas," *IEEE Antennas Wireless Propag. Lett.*, vol. 2, pp. 2–5, 2003.

[28] E. E. Altshuler, "Electrically small self-resonant wire antennas optimized using a genetic algorithm," *IEEE Trans. Antennas Propag.*, vol. AP-50, no. 3, pp. 297–300, Mar. 2002.

[29] R. W. Ziolkowski and A. Kipple, "Application of double negative metamaterials to increase the power radiated by electrically small antennas," *IEEE Trans. Antennas Propag.*, vol. 51, no. 10, pp. 2626–2640, Oct. 2003.

[30] R. W. Ziolkowski and A. D. Kipple, "Reciprocity between the effects of resonant scattering and enhanced radiated power by electrically small antennas in the presence of nested metamaterial shells," *Phys. Rev. E*, vol. 72, p. 036602, Sep. 2005.

[31] R. W. Ziolkowski, "Metamaterials applications to electrically small antennas," in *Proc. IEEE Int. Workshop on Antenna Technology: Small Antennas and Novel Metamaterials*, Singapore, Mar. 7–9, 2005, pp. 7–10.

[32] A. Erentok and R. W. Ziolkowski, "Dipole antennas enclosed in double negative (DNG) and single-negative (SNG) nested spheres: efficient electrically small antennas," in *Proc. IEEE AP-S Int. Symp. and USNC/URSI National Radio Science Meeting*, Washington, DC, Jul. 3–8, 2005.

[33] R. W. Ziolkowski and A. Erentok, "A path to an efficient electrically small antenna: a dipole antenna enclosed in a double negative (DNG) or a single- negative (SNG) metamaterial spherical shell," in *Proc. Symp. on Antennas and Propagation, ISAP2005*, Seoul, South Korea, Aug. 3–5, 2005.

[34] N. Engheta and R. W. Ziolkowski, "A positive future for double negative metamaterials," *IEEE Microwave Theory Tech.*, vol. 53, no. 4, pp. 1535–1556, Apr. 2005.

[35] H. B. Keller and J. B. Keller, "Reflection and transmission of electromagnetic waves by a spherical shell," *J. Appl. Phys.*, vol. 20, pp. 393–396, April 1949.

[36] M. G. Andreasen, "Radiation from a radial dipole through a thin dielectric spherical shell," *IRE Trans. Antennas Propag.*, vol. 5, pp. 337–342, Oct. 1957.

[37] H. R. Raemer, "Radiation from linear electric or magnetic antennas surrounded by a spherical plasma shell," *IRE Trans. Antennas Propag.*, vol. 10, pp. 69–78, Jan. 1962.

[38] R. V. Row, "Radiation efficiency of electric and magnetic dipole antennas surrounded by a small spherical shell of lossy dielectric," *IEEE Trans. Antennas Propag.*, vol. 12, pp. 646–647, Sep. 1964.

[39] D. E. Burrick, "Spheres," in Radar Cross Section Handbook G. T. Ruck, D. E. Barrick, W. D. Stuart, and C. K. Krichbaum, Eds. New York, Plenum Press, 1970, vol. 1, ch. 3.

[40] S. A. Tretyakov, S. I. Maslovski, A. A. Sochaya, and C. R. Simovski, "The influence of complex material coverings on the quality factor of simple radiating systems," *IEEE Trans. Antennas Propag.*, vol. 53, no. 3, pp. 965–970, Mar. 2005.

[41] R. W. Ziolkowski and A. Kipple, "Causality and double-negative metamaterials," *Phys. Rev. E*, vol. 68, p. 026615, August 29, 2003.

[42] L. D. Landau and E. M. Lifshitz, *Electrodynamics of Continuous Media*. Oxford, U.K.: Pergamon Press, 1960, sec. 61–64.

[43] J. Galejs, *Antennas in Inhomogeneous Media*. Oxford, U.K.: Pergamon Press, 1969, ch. 4.

[44] A. Ishimaru, *Electromagnetic Wave Propagation, Radiation, and Scattering*. Englewood Cliffs, NJ: Prentice-Hall, 1991, pp. 288–290.

[45] H. R. Stuart and A. Pidwerbetsky, "Electrically small antenna elements using negative permittivity resonators," presented at the IEEE AP-S International Symp., Washington, DC, Jul. 2005, paper P9.7, unpublished.

[46] K. M. Chen and C. C. Lin, "Enhanced radiation from a plasma-embedded antenna," *Proc. IEEE*, vol. 56, pp. 1595–1597, Sep. 1968.

Richard W. Ziolkowski (M'97–SM'91–F'94) received the Sc.B. degree in physics (*magna cum laude* with honors) from Brown University, Providence, RI, in 1974 and the M.S. and Ph.D. degrees in physics from the University of Illinois at Urbana-Champaign, in 1975 and 1980, respectively.

He was a member of the Engineering Research Division, Lawrence Livermore National Laboratory, CA, from 1981 to 1990, and served as the leader of the Computational Electronics and Electromagnetics Thrust Area for the Engineering Directorate, from 1984 to 1990. He joined the Department of Electrical and Computer Engineering, University of Arizona, Tuscon, as an Associate Professor in 1990, and was promoted to Full Professor in 1996. He was selected by the Faculty to serve as the Kenneth Von Behren Chaired Professor for 2003–2005. His research interests include the application of new mathematical and numerical methods to linear and nonlinear problems dealing with the interaction of acoustic and electromagnetic waves with complex media, metamaterials, and realistic structures.

Prof. Ziolkowski is a member of Tau Beta Pi, Sigma Xi, Phi Kappa Phi, the American Physical Society, the Optical Society of America, the Acoustical Society of America, and Commissions B (Fields and Waves) and D (Electronics and Photonics) of International Union of Radio Science (URSI). He is a Fellow of the Optical Society of America. He was awarded the Tau Beta Pi Professor of the Year Award in 1993 and the IEEE and Eta Kappa Nu Outstanding Teaching Award in 1993 and 1998. He served as the Vice Chairman of the 1989 IEEE/AP-S and URSI Symposium in San Jose, and as the Technical Program Chairperson for the 1998 IEEE Conference on Electromagnetic Field Computation. He served as a member of the IEEE Antennas and Propagation Society (AP-S) Administrative Committee (ADCOM) from 2000–2002. He served as the IEEE AP-S Vice President in 2004 and President in 2005. He is currently serving as a Past-President member of the AP-S ADCOM. He was a Steering Committee Member for the 2004 ESA Antenna Technology Workshop on Innovative Periodic Antennas. He served as a co-Chair of the International Advisory Committee for the inaugural IEEE International Workshop on Antenna Technology: Small Antennas and Novel Metamaterials, IWAT2005, and as a member of the International Advisory Committee for IWAT2006. He was member of the International Advisory Committee for the IEEE 2005 International Symposium on Microwave, Antenna, Propagation and EMC Technologies, MAPE2005. He was an Associate Editor for the IEEE TRANSACTIONS ON ANTENNAS AND PROPAGATION from 1993–1998. He was a co-Guest Editor for the October 2003 IEEE TRANSACTIONS ON ANTENNAS AND PROPAGATION Special Issue on Metamaterials. For the U.S. URSI Society he served as Secretary for Commission B (Fields and Waves) from 1993–1996 and as Chairperson of the Technical Activities Committee from 1997–1999, and as Secretary for Commission D (Electronics and Photonics) from 2001–2002. He served as a Member-at-Large of the U.S. National Committee (USNC) of URSI from 2000–2002 and is now serving as a member of the International Commission B Technical Activities Board. He was a co-Guest Editor of the 1998 special issue of *J. Opt. Soc. Am. A* featuring Mathematics and Modeling in Modern Optics. He was a co-Organizer of the Photonics Nanostructures Special Symposia at the 1998, 1999, 2000 OSA Integrated Photonics Research (IPR) Topical Meetings. He served as the Chair of the IPR sub-committee IV, Nanostructure Photonics, in 2001.

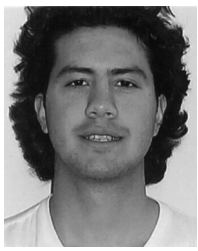

Aycan Erentok received the B.S. (*cum laude* and honors) and M.S. degrees from the University of Arizona, Tuscon, in 2001 and 2003, respectively, all in electrical engineering. He is currently a doctoral student in the Electrical and Computer Engineering Department at the University of Arizona.

His research interests include genetic algorithms, conformal antennas, and the effects of metamaterials on the performance of antennas.

Mr. Erentok received third place in the student paper competition at the 2004 URSI National Radio Science Meeting in Boulder, CO.